ADVANCING A NOVEL CHEMOTYPE FOR THE TREATMENT OF MULTIDRUG - RESISTANT CANCER

A THESIS
SUBMITTED TO THE FACULTY OF
UNIVERSITY OF MINNESOTA
BY

NICHOLAS PAUL BLEEKER

IN PARTIAL FULFILLMENT OF THE REQUIREMENTS
FOR THE DEGREE OF
MASTER OF SCIENCE

Dr. CHENGGUO XING, ADVISER

SEPTEMBER 2013

Acknowledgements

"Research is what I'm doing when I don't know what I'm doing." – Wernher von Braun

It is humbling to reflect on the numerous people who have contributed to my pursuit of higher education. First and foremost, I must acknowledge my research mentor, Dr. Chengguo Xing, who exudes a great passion for making new scientific discoveries that is contagious among his students and research colleagues. His excitement regarding each new experiment was a constant source of motivation during my graduate research and for that I am most grateful. Our relationship has been exceptionally rewarding, and I am confident that the lessons learned during our time together will impact me throughout my professional career.

Second, I am deeply indebted to my family as a constant source of love and support. To my wife, Jonelle, for joining me on the adventure that is graduate school without hesitation and for encouragement when it was needed most. To my parents, Bruce and Brenda, for cultivating my scientific curiosity from a young age, especially by way of a Tasco® microscope kit and telescope; surely these fine instruments were the catalyst for my desire to study that which cannot be seen and to pursue science as a career. Lastly, to my brother, Nathan, who always devoted great effort to his craft and provided inspiration for me to do the same.

I would also like to acknowledge my research colleagues, including past and present members of the Xing lab as well as members of the Thomas lab for their helpful assistance and discussion. In particular, David Hermanson, Bo Zhou, Sonia Das,

Balasubramanian Srinivasan, Aridoss Gopalakrishnan, Sreekanth Narayanapillai, Pablo Leitzman, Manohar Puppala, Xingxin Yu, and Chunlin Zhuang in the Xing lab as well as Tyler Miller and Simon Gruber in the Thomas lab. To varying degrees, each of you has contributed to the work herein. Thank you.

A final acknowledgment is due to the staff and faculty of the medicinal chemistry department for their dedication to the continued success of their students both in the classroom and the laboratory. I would like to especially acknowledge Dr. David D. Thomas, Dr. Carston R. Wagner, and Dr. Daniel A. Harki for serving on my graduate committee and for offering their thoughtful input regarding my research efforts and overall direction. I would also like to thank Dr. Razvan L. Cornea from the Thomas lab for his assistance planning experiments and for constructive conversation.

Dedication

This thesis is dedicated to
Jonelle Alyce Bleeker
for faith in me and in us.

Abstract

Effective cancer treatment is hindered by the onset of drug resistance, regardless of chemotherapeutic agent and its mechanism of action. Both intrinsic and acquired resistance may contribute to the limited efficacy of medicinal agents, presenting a serious challenge for the medical community, including patients, physicians, and scientists. To combat resistant malignancies, scientists have identified Bcl-2 family proteins as key regulators of programmed cell death and strategies to target key members of this family have become a focal point of drug discovery research. Such efforts by members of the Xing lab have led to the development of CXL017, an analogue of sHA 14-1 and novel lead for the treatment of drug-resistant cancers that overexpress antiapoptotic Bcl-2 family proteins. Investigation into the mechanism of action of CXL017 revealed unique biological activity, namely the ability to target several resistant cancer cell types, the ability to re-sensitize HL60/MX2, an acute myeloid leukemia multidrug-resistant cell line, to standard chemotherapeutic agents following long-term, sub-lethal treatment, and the ability to manipulate antiapoptotic Bcl-2 family proteins as well as SERCA, upon re-sensitization. These findings motivated further research regarding this series of compounds. Continued structure-activity relationship studies have led to the development of CXL070, the most advanced CXL to date. Herein, the synthesis and biological evaluation of ten CXL analogues leading to the discovery of CXL070 is reported. In addition, a detailed investigation into the inhibition of SERCA by CXL017 and structurally related analogues provides evidence of a unique binding site within the ER-Ca^{2+} pump. To gain insight into the exact binding site of CXLs within SERCA as

well as enable the discovery of other potential cellular targets via a cell-based pull-down method, the synthesis and utility of a three bifunctional photoaffinity probes based on the CXL scaffold is presented. Preliminary experiments with purified protein and in cells support continued research based on this strategy. Collectively, this work supports the advancement of CXLs as a novel chemotype for the treatment of multidrug-resistant cancer.

Table of Contents

List of Figures

List of Schemes

List of Equations

List of Abbreviations

1DD	DHFR-Gly-DHFR
ABC	ATP-binding cassette
ADR	Adriamycin
ALL	Acute lymphoblastic leukemia
AML	Acute myeloid leukemia
BCA	Bicinchoninic acid
Bcl-2	B-cell lymphoma-2
BH	Bcl-2 homology
BHQ	2,5-di-*tert*-butylhydroquinone
BSA	Bovine serum albumin
c-IAP	C-inhibitor of apoptosis
CML	Chronic myeloid leukemia
CPA	Cyclopiazonic acid
dCK	Deoxycytidine kinase
DHFR	Dihydrofolate reductase
DMSO	Dimethylsulfoxide
DNR	Daunorubicin
DOX	Doxorubicin
ER	Endoplasmic reticulum
FBS	Fetal bovine serum
hHint2	Human histidine triad-nucleotide binding protein

HHT	Homoharringtonine
HRP	Horse radish peroxidase
IP_3R	Inositol triphosphate receptor
MbtI	Mycobacterium tuberculosis salicylate synthase
MDR	Multidrug resistance
MOPS	3-morpholinopropane-1-sulfonic acid
MX	Mitoxantrone
PBST	Phosphate buffered saline TWEEN-20
P-gp	P-glycoprotein
PVDF	Polyvinylidene difluoride
ROS	Reactive oxygen species
SDS-PAGE	Sodium dodecyl sulfate polyacrylamide gel electrophoresis
SEM	Standard error of the mean
SERCA	Sarco/endoplasmic reticulum calcium ATPase
TBTA	Tris-(benzyltriazolylmethyl)amine
TCEP	Tris-(2-carboxyethyl)phosphine
TEM1	β-lactamase (salmonella typimurium)
TG	Thapsigargin
VanX	Vancomycin resistance D-Ala-D-Ala dipeptidase
VLB	Vinblastine

CHAPTER 1

Cancer Drug Resistance: Mechanisms and Therapeutic Strategies

1.1. A need for new cancer therapeutics

Cancer is a collection of diseases typified by dysregulated cell growth that is driven by aberrant gene mutation and expression.[1-3] While genomic changes serve as the root cause of the disease, abnormalities at the molecular level provide the necessary machinery for malignant cells to escape the body's natural defenses and proliferate in a rapid, uncontrolled manner.[4] Cancer is increasingly complex and although new discoveries regarding cancer prevention and treatment are becoming more frequent, the number of cancer-related deaths remains near record highs recorded over the past century. In 1900, cancer was responsible for 64 per 100,000 deaths in the United States. In the year 2000, this number had grown to 200.9 per 100,000.[5] Recent progress involving improved early detection technologies as well as healthier lifestyle choices have driven a decline in the cancer death rate over the past decade.[6] Yet, in 2013, cancer remains the second leading cause of death in this county, accounting for approximately 25% of mortalities.[7] Clearly, much work is yet to be done regarding this devastating disease, but in order to advance the development of novel therapeutics and prevention strategies a deeper understanding of cancer etiology is needed.

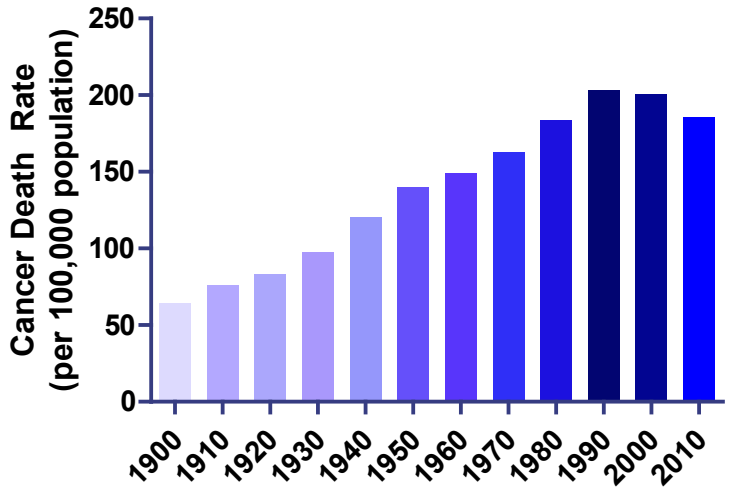

Figure 1.1. Cancer death rates in the U.S. per 100,000 people per year

One of the most pressing challenges in the design of efficacious medicines is drug resistance, as it has a significant effect on therapeutic response and overall patient survival.[8-10] In the case of acute myeloid leukemia (AML), a hematopoietic cancer characterized by irregular proliferation of myeloid precursor cells, drug resistance is especially problematic.[11] Although 50% to 85% of patients achieve remission following standard induction therapy with cytarabine and daunorubicin, the majority of patients undergo relapse and become refractory to standard therapeutic agents (Figure 1.2).[12,13] Often, patients who become refractory to one therapy demonstrate resistance to several therapies, leading to a multidrug-resistant (MDR) state.[14,15] Given the limited treatment options, relapsed disease is often fatal, resulting in death within two years after remission.[11,16] Certainly, there is unmet clinical need for therapies that can eradicate multidrug-resistant AML and improve overall patient survival rates. To address this obstacle, research over the past few decades has led to a better understanding of the

primary mechanisms of drug resistance, providing new avenues for therapeutic intervention.

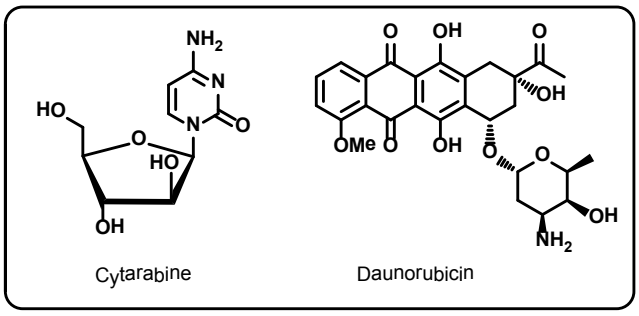

Figure 1.2. Chemical structures of induction chemotherapies for AML

1.2. Mechanisms of drug resistance and the small molecules that target them

Malignant cells employ several mechanisms to evade the toxic effects of chemotherapies. While some mechanisms are specific to a particular drug molecule, other mechanisms endow resistance to a wide range of small molecule therapeutics. Often, drug-specific mechanisms, such as loss of a particular cell-surface receptor, mutation of a specific drug-target, or an alteration to an essential metabolic transformation, can be mitigated by the careful use of drug-combinations.[9] Such cocktails have proven to be extremely useful in the clinic, wherein drugs that rely on different targets and/or biological transformations are dosed together to provide therapeutic diversity and limit the occurrence of resistance.[17] Conversely, non-specific mechanisms of drug resistance are more difficult to address since structurally and functionally unrelated drugs are equally affected, leading to an MDR state that cannot be resolved by straightforward drug substitutions and/or combinations.[18] Two mechanisms contribute to the majority of non-specific drug resistance: the over-expression of drug

efflux pumps and the over-expression of antiapoptotic B-cell lymphoma 2 (Bcl-2) family proteins.[19] Both mechanisms have become the focus of intense drug discovery efforts in order to combat the MDR phenotype (Figure 1.3).

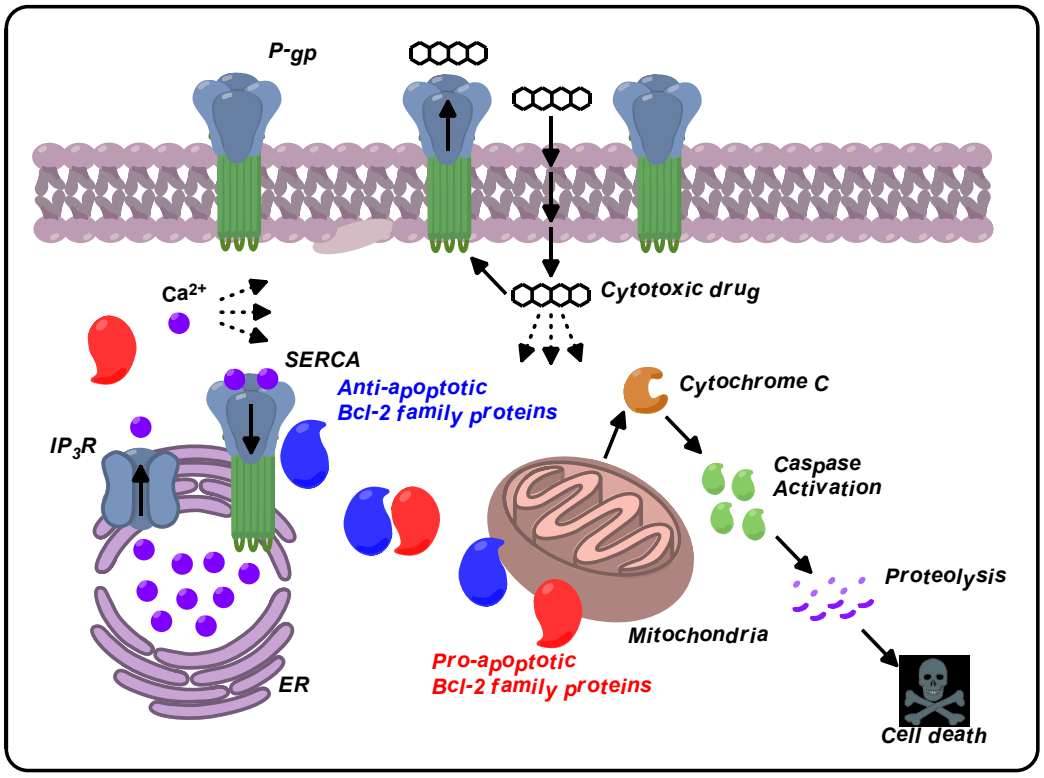

Figure 1.3. General diagram of the cellular function of P-gp and Bcl-2 family proteins as related to drug efflux and mitochondrial cell death

Active drug efflux by ATP binding cassette (ABC)-containing proteins is well-known to lower the accumulation of drugs within tumor cells thereby attenuating any therapeutic benefit.[20,21] Nearly fifty transporters have been identified that carry out this function with each having slightly different structural makeup and substrate specificity.[22] P-glycoprotein (P-gp), also known as MDR1 based on the *MDR1* gene that encodes it or

more formally as ABCB1, is the founding member of the drug efflux transporters.[23] Consisting of two parts each with six transmembrane domains and one ATP-binding site, P-gp is primarily found in the plasma membrane of the intestine, liver, kidney, and blood-brain barrier where it relies on the potential energy of ATP hydrolysis to traffic cytotoxins against their concentration gradient.[24] Importantly, P-gp scavenges a broad range of chemical entities, including those common in chemotherapy regimens.[25,26] In the case of AML, several first line therapies including anthracyclines (daunorubicin, Figure 1.2, and doxorubicin) anthracenes (mitoxantrone), and epipodophyllotoxins (etoposide) are subject to drug efflux by P-gp, resulting in poor therapeutic response and overall clinical outcome (Figure 1.4).

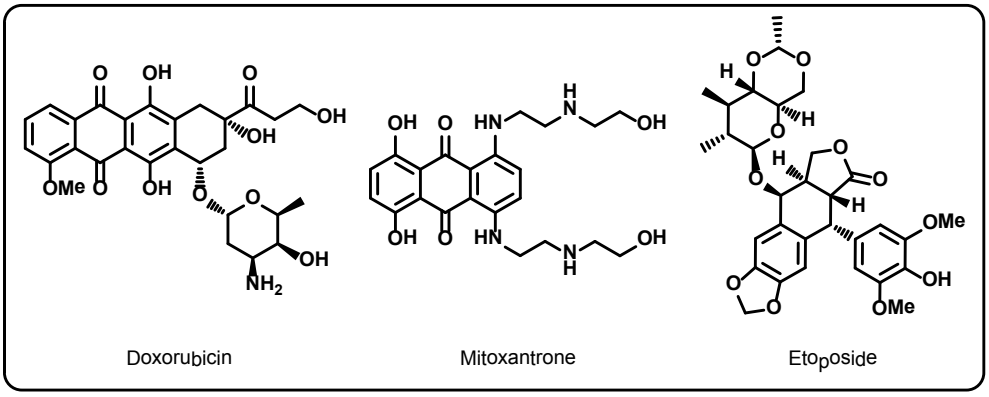

Figure 1.4. Chemical structures of chemotherapies subject to drug efflux

Given the significant clinical impact of this drug transporter, several new and existing drug molecules have been evaluated for their ability to inhibit its action by interfering with ATP (noncompetitive) or substrate (competitive) binding.[27,28] Though first line therapies possessed limited efficacy *in vivo*, second and third generation inhibitors such as PSC-833 (valspodar), XR9576 (tariquidar), and LY335979

(zosuquidar) demonstrate enhanced potency and selectivity for P-gp with improved pharmacokinetic and toxicity profiles (Figure 1.5).[29-31] Clinical evaluation of these compounds is ongoing with modest success reported thus far.[32] In addition, molecules undergoing pre-clinical evaluation, such as isatin-β-thiosemicarbazone developed by Gottesman and co-workers, hold promise as well (Figure 1.5).[33,34] Continued research into the structure and function of P-gp as well as other ABC drug transporters will reveal more effective pharmacological strategies to target efflux-mediated MDR in the future.

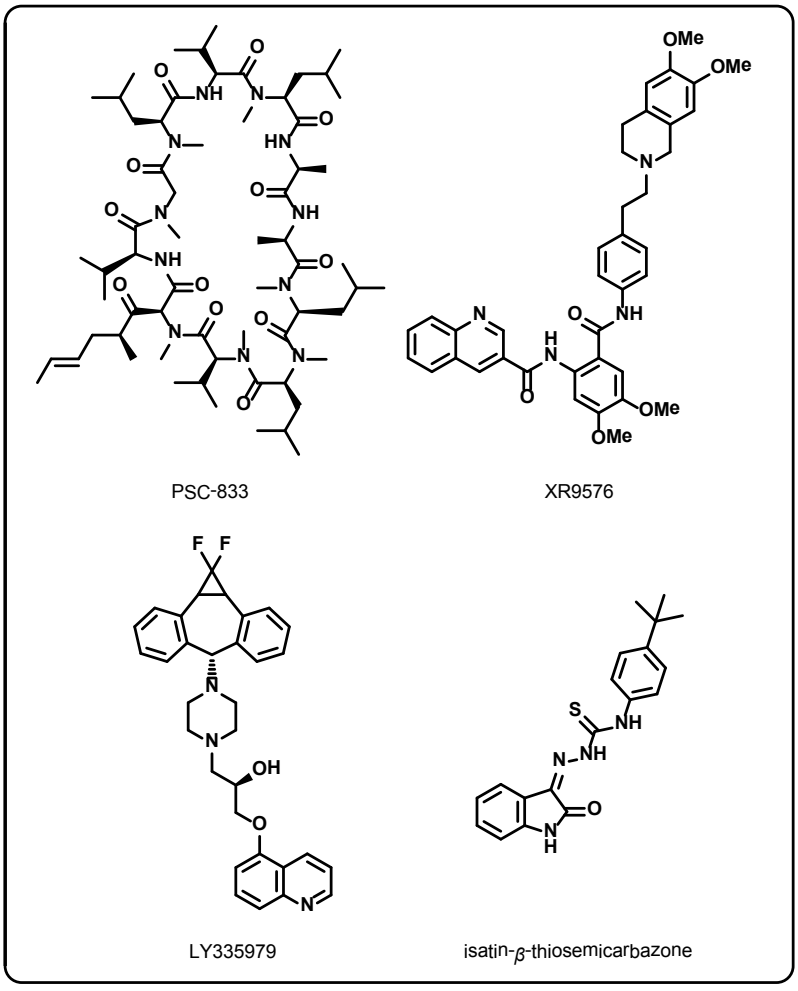

Figure 1.5. Chemical structures of P-gp inhibitors

Unlike active drug-efflux which lowers the drug titer within a malignant cell, over-expression of anti-apoptotic Bcl-2 family proteins lowers the ability of a drug to generate a cell death response.[35,36] Bcl-2 family proteins as a whole consist of both pro- and anti-apoptotic members, which together comprise a dynamic equilibrium that regulates cell fate, primarily at the mitochondria but also at the endoplasmic reticulum (ER).[37-40] Salient anti-apoptotic members include Bcl-2, Mcl-1, and Bcl-X_L whereas classical pro-apoptotic members include Bax and Bak.[41] These well-known Bcl-2 family proteins share three α-helical sequence homology domains referred to as Bcl-2 homology domain 1 (BH1), BH2, and BH3, along with a membrane-anchoring sequence at their C-terminus (Figure 1.6). Uniquely, the anti-apoptotic Bcl-2 proteins contain a fourth homology domain in addition to BH1-3 motifs. A third subset of pro-apoptotic proteins contains only the BH3 domain and includes Bim, Bid, Puma, and Noxa. Although the interplay among the Bcl-2 family is complex, it is generally accepted that antiapoptotic Bcl-2 proteins inhibit cell death by sequestering proapoptotic BH3-only molecules before they can interact with and activate Bax and Bak.[42-44] In the event of apoptotic triggers, activation causes Bax and Bak to undergo homo-oligomerization, which leads to mitochondrial membrane permeablization, cytochrome C release, and caspase activation that ultimately results in cell death. This sequence of mitochondrial events is collectively known as the intrinsic apoptotic pathway (Figure 1.3).[45] At the ER, Bcl-2 family proteins affect calcium homeostasis in part through interaction with the inositol triphosphate receptor (IP_3R) and/or the sarco/endoplasmic reticulum Ca^{2+}-ATPase (SERCA).[46-49] While SERCA is responsible for pumping calcium against its concentration gradient in

order to maintain a ~1000 fold excess (100-500 μM vs. 100 nM) within the ER, IP_3R serves as the primary channel for calcium transport from the ER back into the cytosol.[50] Importantly, regulation of ER calcium flux serves as yet another control point for the execution of cell death, since release of calcium from the ER is implicated upstream of apoptotic events at the mitochondria.[51,52] By controlling apoptotic functions at two organelles, Bcl-2 family proteins serve as a critical factor in regards to the efficacy of most small molecule cancer therapeutics, regardless of mechanism.[53-55]

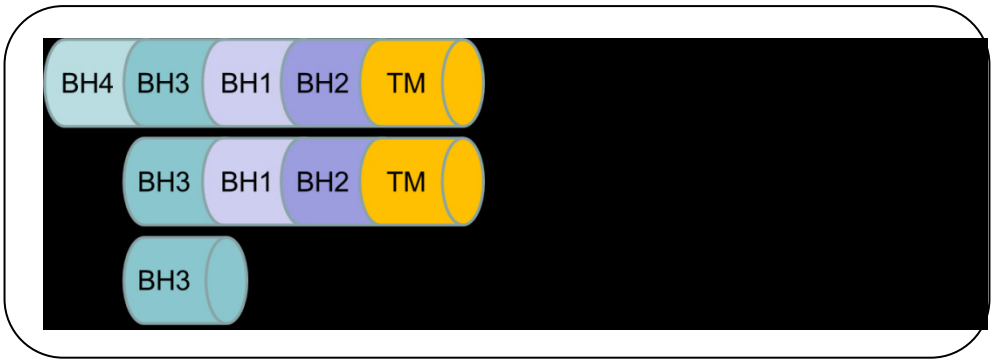

Figure 1.6. Organization of Bcl-2 family proteins according to homology

Both pre-clinical and clinical data support the targeting of anti-apoptotic Bcl-2 family proteins for the development of novel cancer therapies, especially in cases of MDR. Indeed, the over-expression of anti-apoptotic Bcl-2 proteins as well as the reduced expression of pro-apoptotic proteins occurs in both solid and hematological cancers.[56] This altered expression pattern correlates with poor prognosis and reduced therapeutic response, especially among AML patients.[57-59] Analysis of the entire NCI 60 cell line panel, which includes both solid and haemotological cancers, revealed a significant correlation between Bcl-X_L expression and chemosensitivity.[60] In a focused clinical

evaluation, the Bax/Bcl-2 ratio in 255 *de novo* AML patients was shown to directly correlate with complete remission, overall survival, and disease-free survival following treatment with standard induction therapy.[61] Interestingly, recent pre-clinical data points to Mcl-1 as a regulator of mitochondrial calcium signaling and as the critical anti-apoptotic protein in development and maintenance of AML.[62-64] Indeed, there is strong evidence to support the contribution of Bcl-2 family proteins to cancer progression and the occurrence of drug resistance.

With a plethora of reports detailing apoptotic functionality of the Bcl-2 proteins, medicinal chemists have devoted considerable effort to the development of molecules targeting anti-apoptotic family members for cancer therapy. Several compounds have been invented and are at various stages of pre-clinical or clinical evaluation.[65] Based on the discovery that the BH3-only proteins are specific antagonistic ligands of anti-apoptotic Bcl-2 proteins, most inhibitors mimic the pro-apoptotic BH3 domain in order to limit the activity of the anti-apoptotic family members.[66] Advanced clinical examples include GX15-070 and AT-101 from Gemin X Pharmaceuticals (now Cephalon) and Ascenta Therapeutics respectively as well as the ABT compounds 737, 263, and 199, designed in part via structure-activity relationship (SAR) by nuclear magnetic resonance (NMR) from Abbott Labs (Figure 1.7).[67-71] Each of these novel drug entities has enjoyed some success in the clinic, such as GX15-070 in the treatment of refractory AML and ABT-199 in the treatment of refractory chronic lymphoid leukemia (CLL).[72,73] To date, none of these antagonists have received FDA approval; however, it is likely that an anti-apoptotic Bcl-2 inhibitor will advance to the market in the near future.

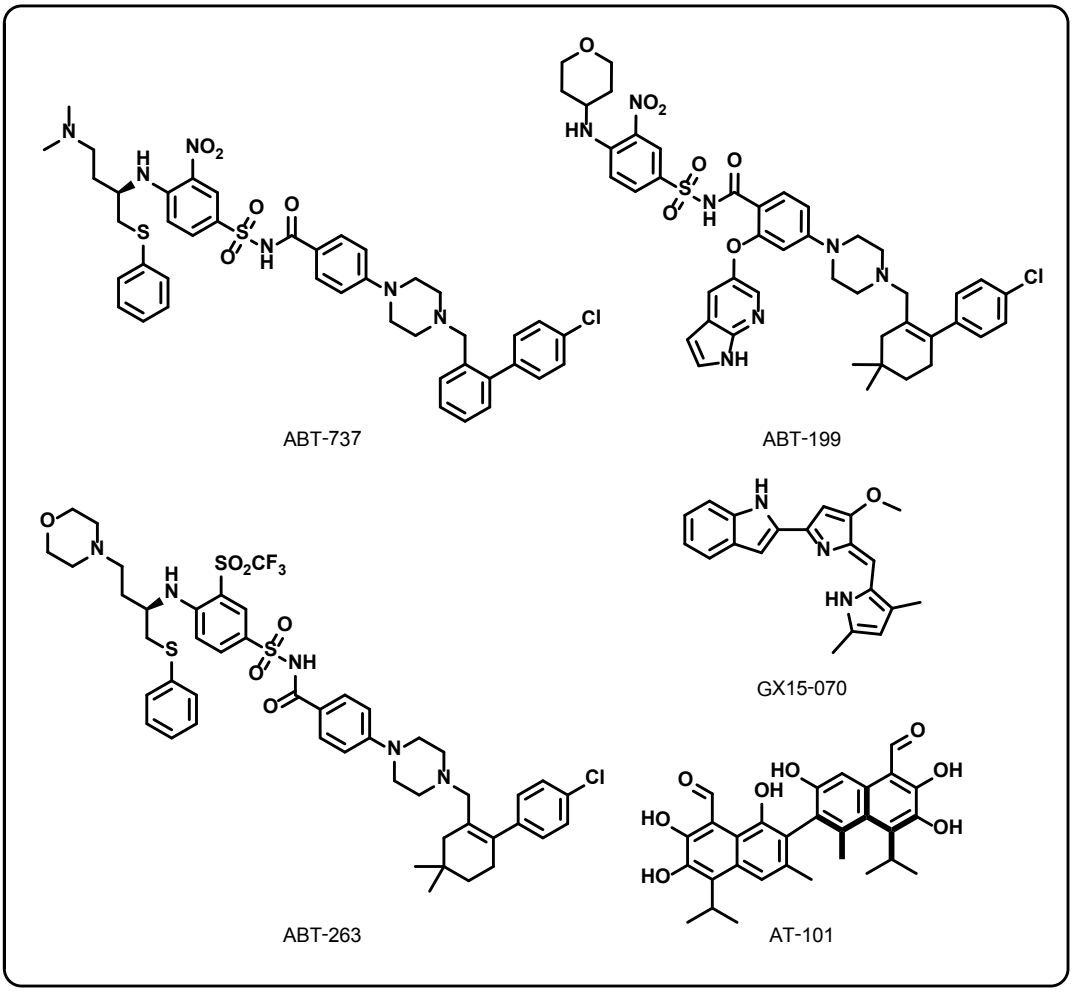

Figure 1.7. Chemical structures of anti-apoptotic Bcl-2 antagonists

1.3. A calcium connection among drug resistance mechanisms

As previously indicated, part of the mechanism by which Bcl-2 family proteins arbitrate cell death is through controlling calcium dynamics at the ER. Calcium is a tightly regulated, secondary cell messenger that participates in a multitude of signaling events related to all aspects of cell physiology.[51,74] At high cytosolic concentrations, calcium becomes toxic to the cell, thus requiring the bulk of the calcium load to be stored

in the ER.[75] Typical signaling events involve transient and localized alterations of cytosolic calcium but in the event of severe cellular stress, emptying of the ER stores can lead to accumulation of calcium at the mitochondria and trigger the aforementioned intrinsic cell death pathway.[76] Consequently, the calcium content of the ER is an important determinant in the cell's sensitivity to apoptosis.[77] In a human cervical cancer cell line (HeLa), genetic down regulation of calreticulin, an ER calcium chaperone, was shown to induce resistance to apoptosis, whereas up-regulation of calreticulin or SERCA both led to apoptotic sensitization.[78,79] It is perhaps not surprising then that Bcl-2 family proteins have dual function at both the ER and the mitochondria in order to control cell fate. In general, anti-apoptotic Bcl-2 proteins limit the accumulation of calcium within the ER whereas pro-apoptotic members, such as Bax, favor increased ER-calcium content, though conflicting reports have failed to detect such effects.[80,81] The exact mechanism of how Bcl-2 proteins regulate the ER calcium load has not been elucidated, but a direct antagonism of SERCA by Bcl-2 is possible based on recent evidence.[49,82] In light of the importance of calcium to the ability of Bcl-2 to oppose cell death, small molecules that interfere with calcium processing may provide a new avenue to target Bcl-2 dependent resistant cancers. For example, separate work by Wong *et al.* and Janssen *et al.* has demonstrated the targeting of apoptosis-resistant cells (Bak/Bax double-knockout murine embryonic fibroblasts) by two different known SERCA inhibitors.[83,84]

In addition to the connection with Bcl-2 family proteins, calcium and calcium-dependent proteins have been associated with P-gp expression and function, indicating a possible link among calcium homeostasis and the two mechanisms of multidrug-

resistance.[85] Calmodulin, a calcium-trafficking protein, was reported to directly interact with P-gp and reduce its drug efflux activity in multidrug-resistant murine erythroleukemia cells.[86] Similarly, genetic down regulation of sorcin, another calcium-binding protein, led to the up-regulation of the *MDR1* gene and subsequent expression of P-gp in HeLa cells.[87] Related work indicated a significant correlation between mRNA expression levels of sorcin and P-gp among 65 AML patients.[88] Moreover, in another murine leukemia cell line (L1210/VCR) the over-expression of P-gp was associated with the reduction in SERCA2 levels.[89] By comparing this resistant cell line with its parental counterpart (L1210), uptake of radioactive calcium-45 was found to more effective in P-gp positive cells compared to P-gp negative cells.[90] While the elucidation of the complete network of calcium dynamics as it relates to P-gp in drug resistance is ongoing, preliminary evidence indicates a potential role for calcium modulators to mitigate resistant cancers. In particular, inhibition of SERCA, the ATP-dependent ER calcium pump, provides an attractive point of intervention, as it is implicated in P-gp and Bcl-2-mediated mechanisms of non-specific multidrug-resistance.

Several SERCA inhibitors have been identified with diverse chemical structures, binding affinities, and biological activities.[91] The more potent inhibitors have been implemented to study the influence of calcium signaling on aspects of cell physiology and have proven most useful in the determination of high-resolution structures of inhibitor-bound forms of the ATPase (Figure 1.8).[92-94] Such inhibitors include thapsigargin (TG), cyclopiazonic acid (CPA), and 2,5-di-*tert*-butylhydroquinone (BHQ), all possessing submicromolar dissociation constants.[95] By far the most widely utilized,

TG is a sesquiterpene lactone that binds the E2 form of the enzyme in the transmembrane (TM) domain.[96] Similarly, CPA and BHQ also bind the E2 form of SERCA at a well-characterized site in the TM domain, though with weaker binding affinity than TG.[97,98] The CPA binding site is distinct from that of TG but partially overlaps with the BHQ site.[95] To date, only TG and related derivatives have been implemented in the clinic as a result of dose-limiting toxicity.[99-101] However, a recent discovery by Roti *et al.* demonstrating SERCA as an up-stream regulator of Notch1 and the ability of TG to successfully target *NOTCH1* mutated leukemia *in vivo*, encourages further research into new and existing SERCA inhibitors for certain cancer types.[102] Perhaps the clinical potential of SERCA inhibitors will not be realized without the advent of new chemotypes that avoid the toxicity issues associated with thapsigargin.

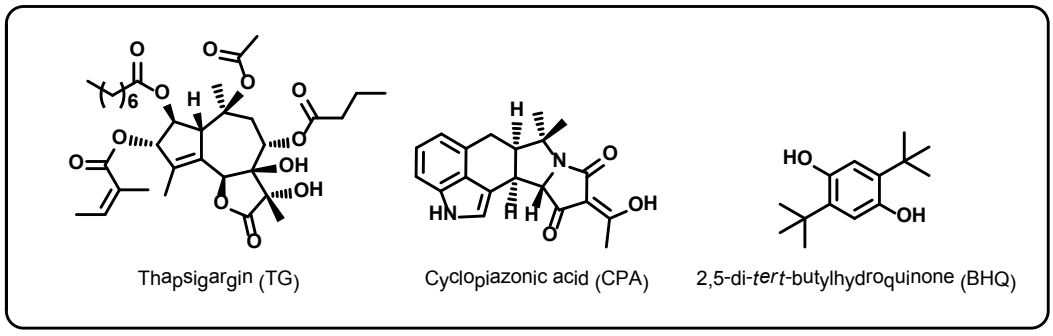

Figure 1.8. Chemical structures of SERCA inhibitors

1.4. The development of CXL017

Over the past decade, research in the Xing lab has focused on the development of a series of compounds with the ability to target multidrug-resistant cancers (Figure 1.9). Rigorous structure-activity relationship studies over the better part of a decade have led

from HA-14-1 a putative Bcl-2 inhibitor identified from a computer-aided screen, to sHA 14-1, a stable and reactive oxygen species (ROS)-free derivative, to CXL017, a superiorly potent molecule compared to sHA 14-1 when evaluated across a panel of cancer cell lines.[103-105] During the course of experimentation leading to the discovery of CXL017, considerable insight into the mechanism of sHA 14-1 was gained. Importantly, sHA 14-1 was shown to act on both the mitochondria and ER in order to elicit its cytotoxic effect.[106] In a human leukemia cell line (NALM-6), sHA 14-1 induced mitochondrial membrane depolarization in addition to ER calcium release, which could be attributed to direct antagonism of SERCA and not IP_3R. Furthermore, sHA 14-1 retained the ability to target antiapoptotic Bcl-2 family proteins, similar to its predecessor, HA 14-1.[107] Together, these findings sparked excitement regarding further development of this series of molecules. Unfortunately, sHA 14-1 demonstrated limited efficacy *in vitro*, thus motivating further optimization of the lead compound.

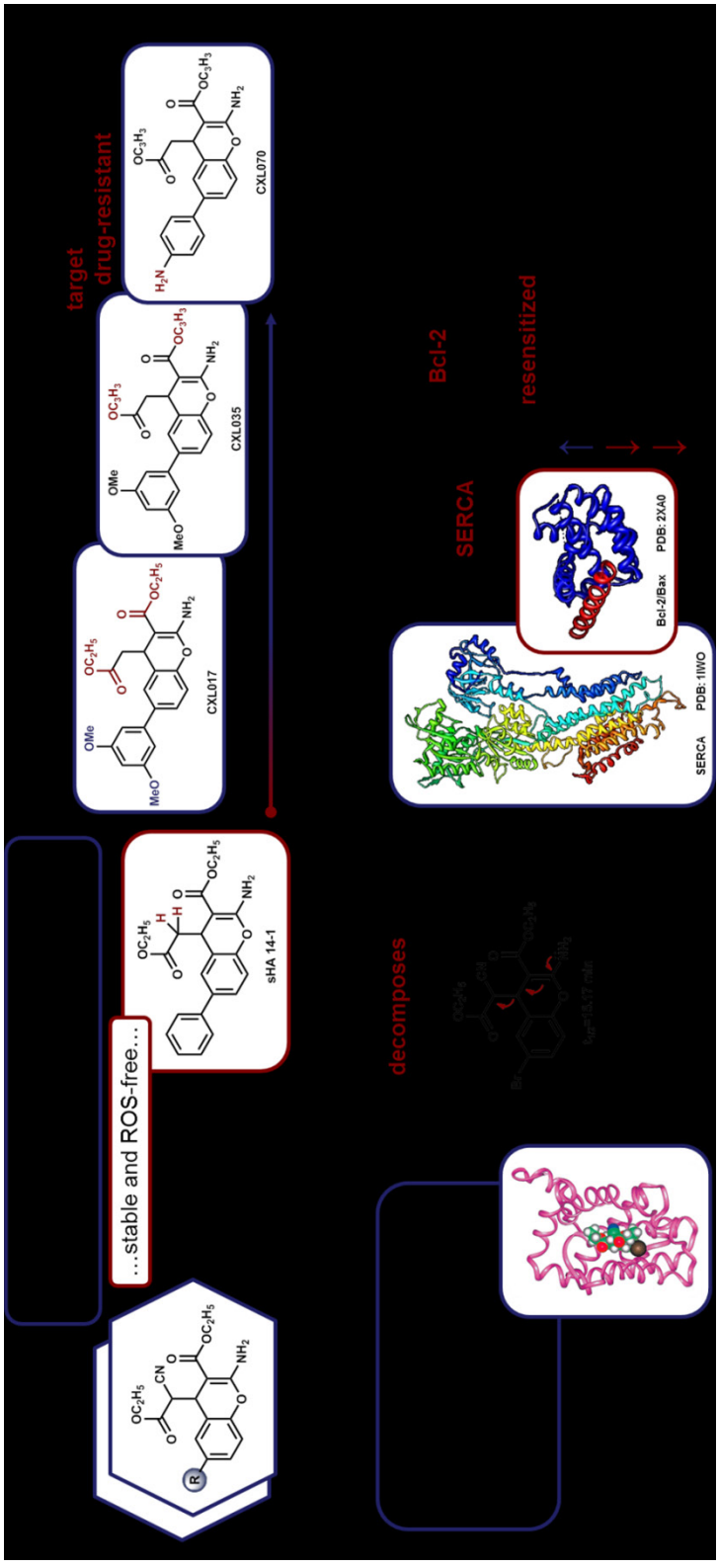

Figure 1.9. Timeline of the development of the CXL series

Rigorous structure-activity relationship studies culminated in the discovery of CXL017 as an advanced small molecule for the treatment solid and haematologic cancers following cytotoxicity evaluation in several cancer cell lines including the NCI-60 cell line panel.[108] Furthermore, CXL017 exhibited the ability to synergize with standard chemotherapeutic agents and target drug-resistant leukemic cells (CCRF-CEM/C2 and HL60/MX2) over parental cells (CCRF-CEM and HL60). Results of an *in vivo* study provided further evidence for the ability of CXL017 to target HL60/MX2-derived tumors compared to HL60-derived tumors.[109] Given its ability to mitigate MDR, experimentation was undertaken to evaluate the ability of HL60 or HL60/MX2 cells to develop resistance to CXL017. Following chronic treatment for six months with sub-lethal doses of CXL017, both parental and resistance cell lines failed to develop stable resistance to CXL017.[109] Because of possibility of MDR occurring during long-term treatment, sensitivity to standard therapies was re-evaluated, and excitingly, HL60/MX2 cells demonstrated sensitization to three standard therapeutic agents, namely cytarabine, doxorubicin, and mitoxantrone. This re-sensitization was stable following removal of CXL017, indicating that continuous treatment was not necessary to retain the sensitive phenotype. Exploration into the cause of re-sensitization revealed altered levels of Mcl-1, Bax, Bim, Noxa, and SERCA proteins as well as a diminished ER calcium load.[109] Drug efflux was proven to not play a role in the re-sensitization induced by CXL017. Collectively, the experimental data surrounding CXL017 cultivated great interest in the further development of this series of compounds for the treatment of MDR leukemia.

Continued research into the mechanism of action of CXL017 and the synthesis of novel chemotypes to exploit said mechanistic insights proved exceptionally motivating for one young scientist. The following is this author's contribution to the advancement of the CXL series for the treatment of multidrug-resistant cancer.

CHAPTER 2*

New Analogues of CXL017

2.1. Introduction

As a potential lead for the treatment of MDR cancer, CXL017 demonstrated relatively weak, low-micromolar potency when evaluated *in vitro*, a limiting factor with respect to further advancement. In order to improve the potency of CXL017, additional structural modifications of the 4*H*-chromene system were explored by employing a customary synthetic route.[104,105,110] An impressively narrow structure-activity relationship resulted in the placement of optimal functionalities at the 3, 4, and 6 positions of the core scaffold (Fig. 2.1). Accordingly, these efforts led to the identification of several candidates with submicromolar cytotoxicity towards HL60, a parental AML cell line. From this initial screen, CXL070 emerged as a superior lead molecule compared to CXL017. Following the characterization of nine MDR leukemic cell lines, the scope of CXL070 was explored. CXL070 demonstrated equipotent or superior activity in all nine MDR cell lines compared to the respective parental cell lines. In comparison to small molecules that target antiapoptotic Bcl-2 family proteins (ABT-737), SERCA (thapsigargin), or P-gp (isatin-β-thiosemicarbazone), CXL070 demonstrated the greatest ability to target MDR cells among all four compounds, validating its prescribed evaluation *in vivo*.

---

*Part of this chapter have been reproduced with permission from Das, S. G. *et al.* Structure-activity relationship and molecular mechanisms of ethyl-2-amino-6-(3,5-dimethoxyphenyl)-4-(2-ethoxy-2-oxoethyl)-4*H*-chromene-3-carboxylate (CXL017) and its analogues. *J. Med. Chem.* **54**, 5937-5948 (2011).

Aridoss, G. *et al.* Structure−activity relationship (SAR) study of ethyl 2-Amino-6-(3,5-dimethoxyphenyl)-4-(2-ethoxy-2-oxoethyl)-4*H*-chromene-3-carboxylate (CXL017) and the potential of the lead against multidrug resistance in cancer treatment. *J. Med. Chem.* **55**, 5566-5581 (2012).

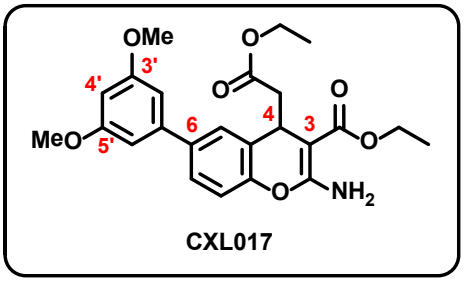

Figure 2.1. Chemical structure of CXL017 with atom numbering

2.2. Results and Discussion

2.2.1. Design and synthesis of novel CXL analogues (performed together with Dr. Balasubramanian Srinivasan and Dr. Aridoss Gopalakrishnan)

Previous experimental results indicated that the activity of CXL candidates is particularly sensitive to the functional groups at the 3 and 4 positions.[105] Here, the preferred balance of size, lipophilicity, and flexibility at these two positions was further characterized. In general, synthesis commenced via a Suzuki-Miyaura coupling reaction between 5-bromosalicylaldehye and an appropriate boronic acid to yield the corresponding 5-aryl salicylaldehyde. Subsequent transformation with *N*,*N*-dimethylacetamide and $POCl_3$ furnished the intermediate coumarin in good yields, which could be carried on to the final stage upon reaction with methyl (CXL093 only) or ethyl cyanoacetate in the presence of various sodium alkoxides generated *in situ* (Scheme 2.1). Overall yields of this final elaboration typically ranged from 45% to 60%, but proved exceptionally sluggish depending on the selection of alcohol. To afford the

dioxirane methyl derivative, CXL086, standard epoxidation conditions with *m*-CPBA were utilized (Scheme 2.2).

Scheme 2.1. General synthetic route for the preparation of CXL analogues

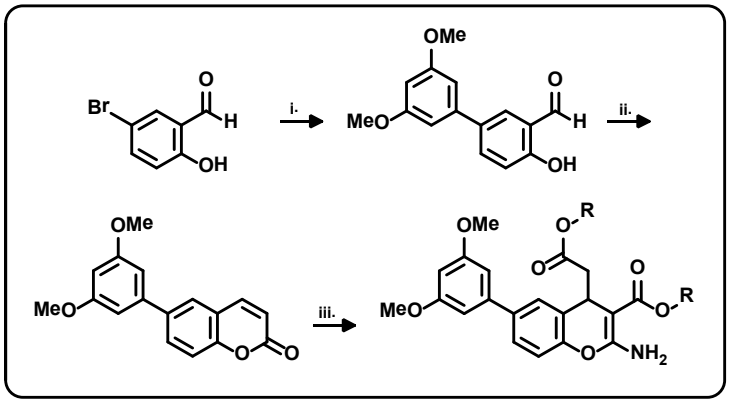

Reagents and conditions: (i) $ArB(OH)_2$, $Pd(OAc)_2$, PPh_3, K_2CO_3, DMF:H_2O, 80 °C, 16 h; (ii) DMA, $POCl_3$, DCM, 0 °C to 80 °C, 4 h, $NaHCO_3$, 60 °C, 1 h; (iii) Methyl or ethyl cyanoacetate, NaOR, ROH, rt, 3h.

Scheme 2.2. Final synthetic transformation for CXL086

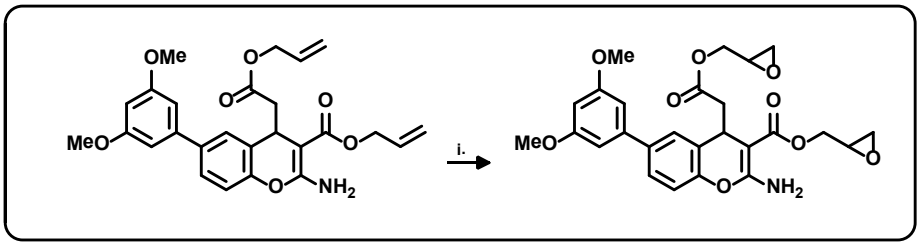

Reagents and conditions: (i) *m*-CPBA, DCM, 0 °C to rt, 24 h

Additional earlier studies suggested that the 3' and 4' positions of the 6-phenyl group are critical to the potency of CXL candidates. Consequently, functionalization of

each of these positions with a methoxy or a methyl improved activity, whereas functionalization at both positions led to significant loss of activity. To further explore the SAR at these positions, a series of amino-functionalized analogues at the indicated positions were prepared. Preparation of primary amine-substituted derivatives commenced via Suzuki coupling of a nitro-substituted arylboronic acid with 5-bromocoumarin (synthesized from 5-bromosalicyladeyde) followed by Pd/C-catalyzed reduction of the nitro functionality to furnish the desired aminocoumarins. Final conversion to the target 4*H*-chromenes was carried using the procedure highlighted above (Scheme 2.3).

Scheme 2.3. Synthetic route for CXL055 and CXL070

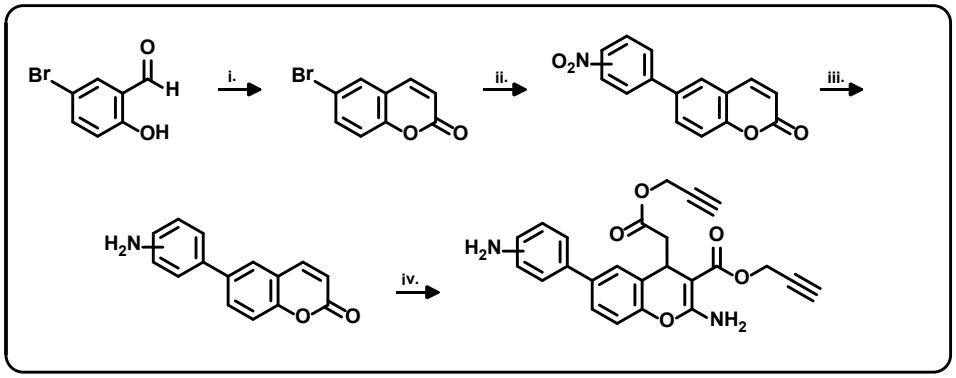

Reagents and conditions: (i) DMA, $POCl_3$, DCM, 0 °C to 80 °C, 4 h, $NaHCO_3$, 60 °C, 1 h; (ii) $ArB(OH)_2$, $Pd(PPh_3)_4$, K_2CO_3, Toluene:H_2O, 80 °C, 16 h; (iii), Pd/C (10%), NH_4CO_2, MeOH, 6 h, rt (iv) Ethyl cyanoacetate, NaOR, ROH, rt, 3h.

2.2.2. *In vitro* cytotoxicity of new CXL analogues (performed by Dr. David Hermanson and Dr. Chengguo Xing)

The biological activity of these small molecules was first evaluated in HL60 following a well-established procedure, since this parental line is typically less sensitive to CXL candidates when compared to the resistant cell line, HL60/MX2 (Table 2.1).[105] The cytotoxicity results illustrated that the functional groups at the 3 and 4 positions are especially important to the observed activity. Indeed, there was a 13-fold difference in cytotoxicity between the methyl (CXL093) and the *n*-butyl (CXL042) analogues with the ethyl (CXL017) and *n*-propyl (CXL041) analogues in between. Reduction in flexibility at these positions improved activity. This was reflected by the dipropargyl esters (CXL035) being 3 and 5 times more potent than the diallyl (CXL042) and di-*n*-propyl (CXL041) compounds, respectively.

With the preference for dipropargyl moieties at the 3 and 4 positions, the preferred amino substitution at the 3' and 4' positions of the 6-aryl ring was determined (Table 2.1). The 4' amino derivative (CXL070) lacking any further substitution provided the greatest enhancement in activity with an IC_{50} of 0.61 ± 0.08 μM in HL60 cells, two-fold more potent than the 3' substituted analogue (CXL055). Of note, several derivatives with changes to the 6-aryl potion of the molecule were prepared by variation on the aforementioned synthetic route. Proving to be most active compounds, only the primary amino derivatives are discussed herein.

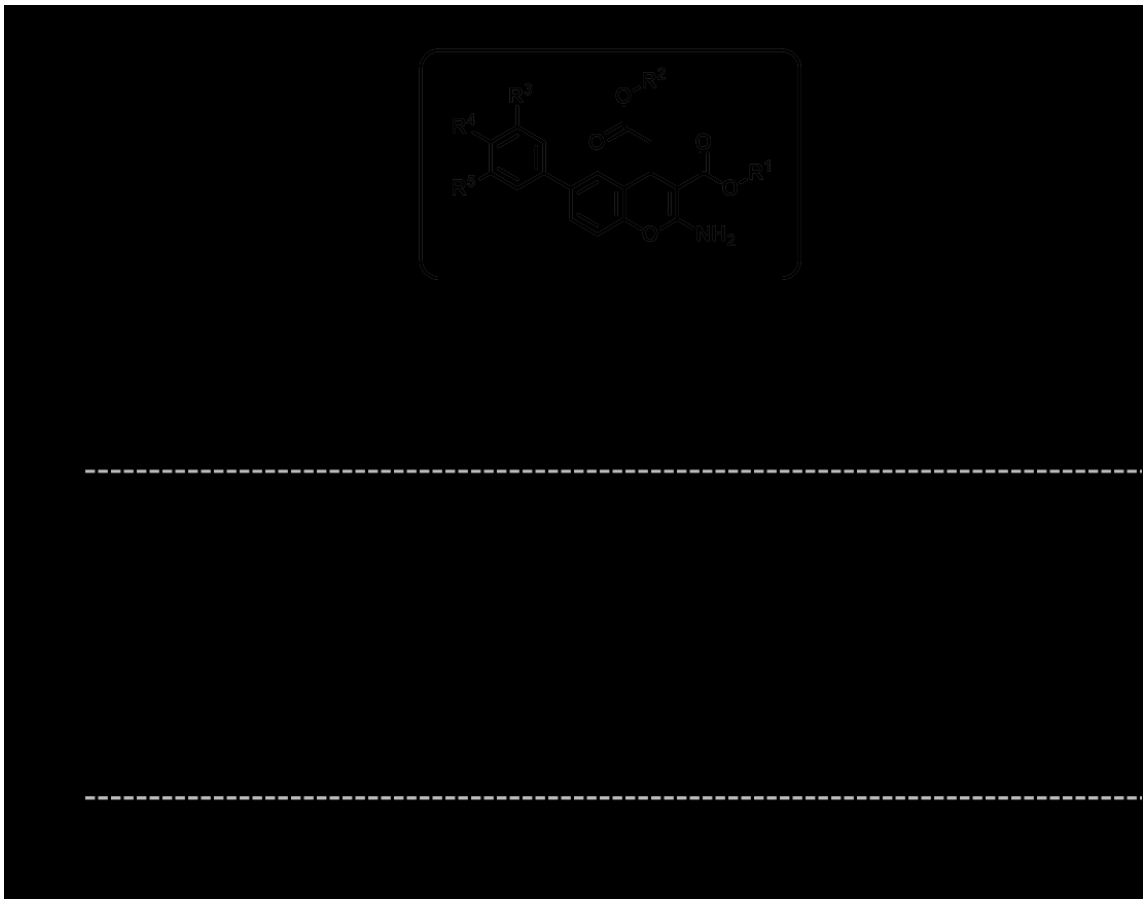

Figure 2.2. Cytotoxicity of CXLs in HL60 cells. CXLs were evaluated in a cell viability assay at various concentrations in HL60 cells. (A) CXL chemical scaffold. (B) The IC_{50} (μM) of each analogue was determined from the fit of a dose-response curve to the four-parameter dose-response equation (Eq. 2.1). Data are expressed as mean ± SEM, n = 3 with triplicate data points in each experiment.

2.2.3. Characterization of nine parental and MDR cancer cell lines (performed by Dr. David Hermanson and Dr. Chengguo Xing)

In order to evaluate the scope of CXL070 against MDR in cancer treatment, several pairs of resistant and parental cancer cell lines were obtained: four pairs of AML

(HL60 vs HL60/MX2, HL60/ADR, HL60/DNR, and HL60/DOX), three pairs of ALL (CCRF-CEM vs CCRF-CEM/C2, CCRF-CEM/VM-1-5, and CCRF-CEM/VLB100), and two pairs of CML (K562 vs K562/DOX and K562/HHT300). The MDR cell lines were developed from the parental cell lines through chronic exposure to different cancer therapies, including mitoxantrone (a topoisomerase II inhibitor, MX2), doxorubicin/adriamycin (a topoisomerase II inhibitor, DOX/ADR), daunorubicin (a topoisomerase II inhibitor, DNR), camptothecin (a topoisomerase I inhibitor, C2), homoharringtonine (an antimitotic agent, HHT), and vinblastine (an antimitotic agent, VLB). Several of these cancer therapies are the first- or second-line therapies against AML, ALL, and/or CML, substantiating the clinical relevance of these MDR cancer cell line models. These cell lines acquire MDR through different mechanisms. For instance, the apoptotic machinery is impaired in HL60/DOX via the up-regulation of c-inhibitor of apoptosis (c-IAP).[111] HL60/MX2 confers its resistance against mitoxantrone via down-regulating of topoisomerase IIβ with no involvement of p-glycoprotein.[112,113] CCRF-CEM/C2 and CCRF-CEM/VM-1-5 gain resistance via target mutation.[114-116] HL60/MX2 and CCRF-CEM/C2 also have elevated levels of antiapoptotic Bcl-2 family proteins.[105] On the other hand, HL60/ADR, HL60/DNR, K562/DOX, K562/HHT300, and CCRF-CEM/VLB100 all mediate their resistance at least partially via the overexpression of P-gp.[117,118]

This set of parental and MDR cell lines were evaluated for their sensitivity against a panel of standard therapies in a dose-dependent manner to determine the IC_{50} values. The ratio of the IC_{50} in the MDR cell line relative to the IC_{50} in the parental cell line

provided a clear representation of the cross-resistance of each cell line (Figure 2.2). As expected, the MDR cell lines generally demonstrate cross-resistance to standard cancer therapies. Since several of these (HL60/MX2, HL60/ADR, HL60/DNR, HL60/DOX, K562/DOX, and CCRF-CEM/VM-1-5) acquire their resistance through exposure to topoisomerase II inhibitors, they all demonstrate significant cross-resistance to doxorubicin, mitoxantrone, and etoposide, three topoisomerase II inhibitors. Similarly, K562/HHT300 demonstrates significant cross-resistance to vincristine given that its resistance was developed upon exposure to an antimitotic agent. CCRF-CEM/C2, however, reveals no or weak cross- resistance toward the therapies evaluated. This is reasonable, since its resistance was developed upon target mutation following exposure to camptothecin, a topoisomerase I inhibitor.[42,114] There are three additional interesting observations. First, HL60/ADR and HL60/DOX both are derived from HL60 upon exposure to the same topoisomerase II inhibitor, doxorubicin. Yet, each reveals a distinct drug sensitivity profile in that HL60/DOX demonstrates a greater extent of cross-resistance compared to HL60/ADR. Several factors may contribute to the difference among these cell lines, such as dissimilar treatment regimens during the development of resistance. Second, these resistant cell lines reveal either substantial (>1000-fold) or no resistance to vincristine. From the reported characterization of these cell lines, HL60/DNR, K562/DOX, K560/HHT300, and CCRF-CEM/VLB100 all overexpress P-gp while HL60/DOX has not been well characterized for this protein. Since vincristine is an excellent substrate for drug efflux, P-gp overexpression is a likely mechanism of resistance for this particular small molecule. Third, none of these MDR cell lines reveals

>10-fold resistance to cytarabine. In fact, two cell lines reveal collateral sensitivity to this anti-metabolic agent. These data suggest that cytarabine is less likely to suffer cross-resistance that originates from mechanistically unrelated cancer therapies, consistent with the reported mechanism of cytarabine-resistance - reduction in the activity of deoxycytidine kinase (dCK), an enzyme involved in the rate limiting step for cytarabine activation, which is unlikely to change in these MDR cancer cells.[119] Together, the mechanistic diversity among these MDR cell lines provided an excellent system to evaluate the utility of the new lead compound, CXL070.

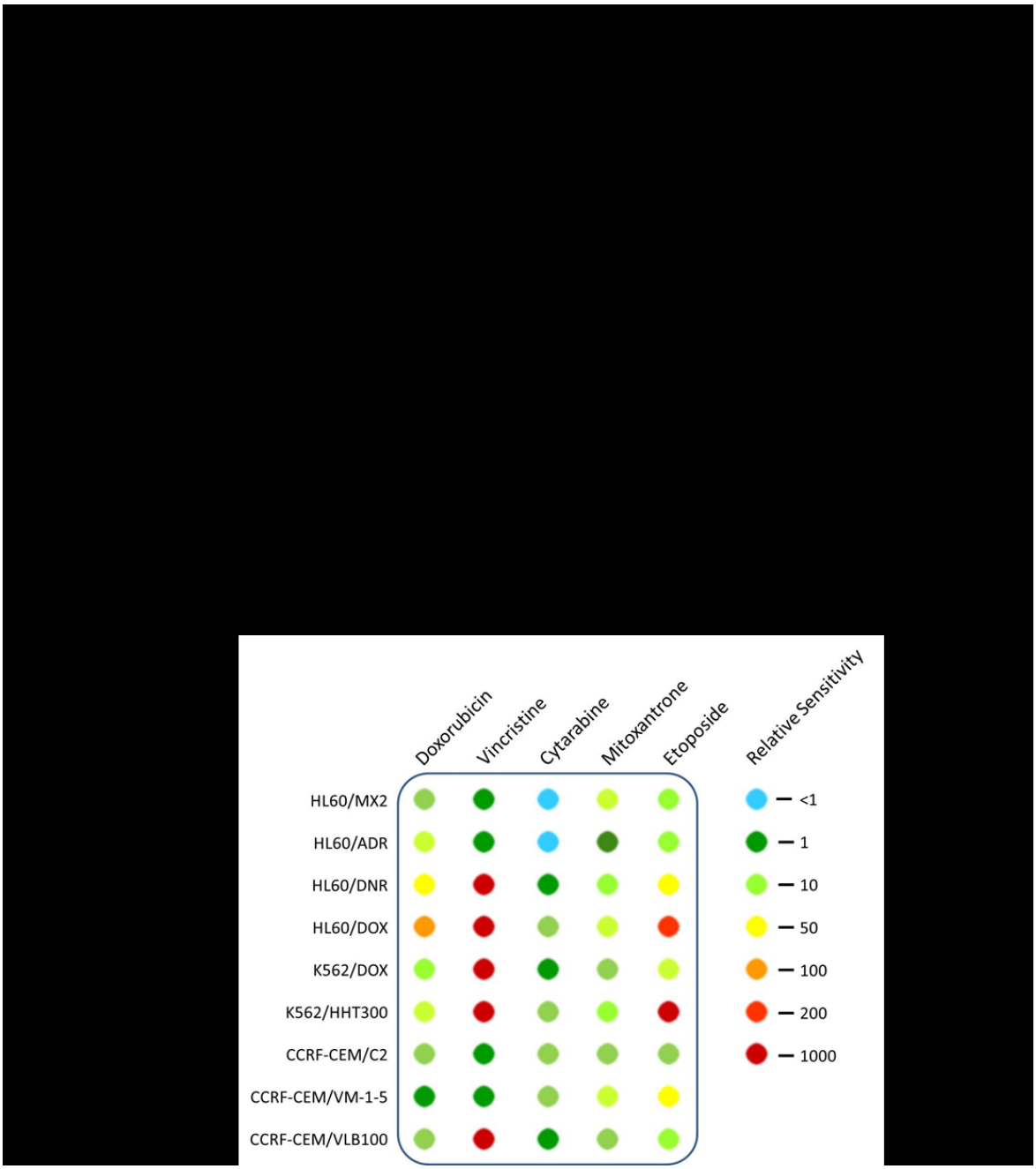

Figure 2.3. Relative sensitivity of MDR cancer cells towards standard therapies. Doxorubicin, vincristine, cytarabine, mitoxantrone, and etoposide were evaluated in a cell viability assay at various concentrations in MDR and parental cell lines. The IC_{50} of each compound was determined from the fit of a dose-response curve to the four-parameter

dose-response equation (Eq. 2.1). Relative sensitivity is defined as the ratio of the IC_{50} in the resistant cell line relative to that in the corresponding parental cell line. Relative sensitivity >1 indicates resistance whereas sensitivity <1 indicates collateral sensitivity. (A) Relative sensitivity and the IC_{50} of standard therapies in parental cell lines. (B) Heat map derived from data in A. Data are expressed as mean ± SEM, n = 2 with triplicate data points in each experiment. Since these cell lines originiate from different sources (see Section 2.4), the parental cell lines with the same designation do not demonstrate equialent sensitivity to the same therapeutic agent.

2.2.4. Sensitivity profiling of nine parental and MDR cancer cell lines to MDR targeting agents (performed by Dr. David Hermanson and Dr. Chengguo Xing)

ABT-737, isatin-β-thiosemicarbazone, and thapsigargin target Bcl-2 family proteins, P-gp, or SERCA respectively.[34,71,100] Along with CXL070, these four compounds were evaluated for their cytotoxicity against the parental and MDR cell lines in a dose-dependent manner to determine their ability to target MDR cancer cells (Figure 2.3). Again, the ratio of the IC_{50} in the MDR cell line relative to the IC_{50} in the parental cell line for each inhibitor was determined (Figure 2.3). With respect to ABT-737, seven of the nine MDR cell lines revealed 2- to 20-fold resistance and two cell lines, CCRF-CEM/C2 and CCRF-CEM-VLB100, revealed significant collateral sensitivity. These data indicated that targeting the antiapoptotic Bcl-2 family proteins alone, was not sufficient to overcome MDR within this panel of cell lines. Consistent with the results reported by Gottesman *et al.* in other MDR models, MDR cancer cells that overexpress

P-gp, such as HL60/ADR, HL60/DNR, K562/DOX, K562/HHT300, and CCRF-CEM/VLB100, were collaterally sensitivity to isatin-β-thiosemicarbazone.[33,34] CCRF-CEM/C2 cells also showed collateral sensitivity to the efflux inhibitor, though its ability to accumulate camptothecin has been reported to be on par with the parental cell line, signifying a lack of P-gp involvement.[120] HL60/MX2, HL60/DOX, and CCRF-CEM/VM-1-5 failed to show collateral sensitivity to isatin-β-thiosemicarbazone, given that they acquire resistance independent of P-gp. Indeed, CCRF-CEM/VM-1-5 revealed a 2-fold resistance to the P-gp inhibitor. In the case of thapsigargin, six of the nine MDR cell lines conferred cross-resistance, while HL60/MX2 demonstrated significant (>50-fold) collateral sensitivity. Finally, for CXL070, five of the nine MDR cell lines showed collateral sensitivity, and none of them demonstrated any resistance. Since these cells acquire MDR through several mechanisms, these results support the hypothesis that CXL070 targets several key components of the resistance machinery and that cancer cells are unlikely to acquire resistance to CXL070, especially in comparison to ABT-737, thapsigargin, and isatin-β-thiosemicarbazone.

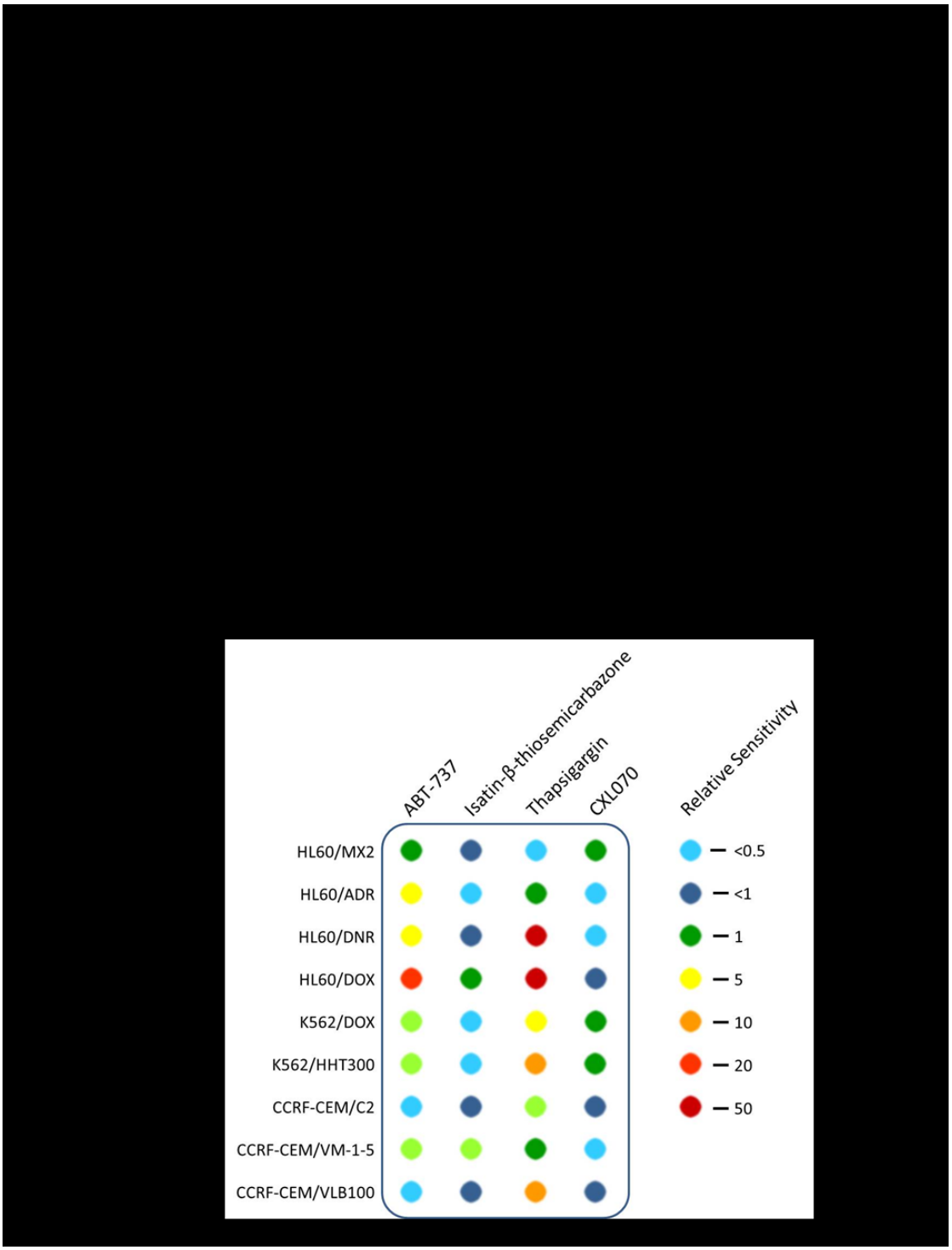

Figure 2.4. Relative sensitivity of MDR cancer cells towards MDR targeting agents. ABT-737, isatin-β-thiosemicarbazone, thapsigargin, and CXL070 were evaluated in a cell viability assay at various concentrations in MDR and parental cell lines. The IC_{50} of each

compound was determined from the fit of a dose-response curve to the four-parameter dose-response equation (Eq. 2.1). Relative sensitivity is defined as the ratio of the IC_{50} in the resistant cell line relative to that in the corresponding parental cell line. Relative sensitivity >1 indicates resistance whereas sensitivity <1 indicates collateral sensitivity. (A) Relative sensitivity and the IC_{50} of MDR inhibitors in parental cell lines. (B) Heat map derived from data in A. Data are expressed as mean ± SEM, n = 2 with triplicate data points in each experiment. Since these cell lines originiate from different sources (see Section 2.4), the parental cell lines with the same designation do not demonstrate equialent sensitivity to the same therapeutic agent.

2.3. Conclusion

Based on the potential of CXL017 to target MDR, a detailed SAR study was undertaken to characterize the optimal functional groups at the 3, 4, and 6 positions of the 4*H*-chromene system. The 3 and 4 positions proved quite sensitive to the size, flexibility, and lipophilicity of the functional groups with propargyl esters being preferred (Table 2.1). Increasing flexibility or hydrophilicity significantly reduced the cytotoxicity of the molecules towards HL60. The functional groups at the 3' and 4' positions of the 6-aryl system also significantly affected the resultant cytotoxicity of newly synthesized analogues (Table 2.1). In general, only small and hydrophilic substitutions were tolerated at these positions. The outcome of the SAR study led to the discovery of CXL070 with an IC_{50} of 600 nM against HL60 cells, approximately 20 times more potent than its predecessor, CXL017. With a new lead compound in-hand, the ability of CXL070 to

target multiple MDR cell lines was determined alongside inhibitors of known resistance mechanisms.

Among the small molecules evaluated including ABT-737, isatin-β-thiosemicarbazone, and thapsigargin, CXL070 proved to be the most efficacious small molecule against MDR, as no cross-resistance was observed in any of the cell lines tested. Interestingly, five of the nine MDR cell lines, harboring different resistance mechanisms, displayed collateral sensitivity toward CXL070. With unique resistance mechanisms ranging from the overexpression of antiapoptotic Bcl-2 family proteins (CCRFCEM/C2), to the overexpression of P-gp (HL60/ADR and HL60/DNR), to an apoptotic defect downstream of the mitochondrial Bcl-2 family proteins (HL60/DOX), as well as target mutation (CCRF-CEM/VM-1-5 and CCRF-CEM/C2), this subset of MDR cell lines encourage further scientific research, especially *in vivo* evaluation, of this new lead compound for the treatment of MDR cancer.

2.4. Materials and Methods

2.4.1. Chemistry

All commercial reagents and anhydrous solvents were purchased from vendors and were used without further purification or distillation unless otherwise stated. Analytical thin layer chromatograph was performed on Whatman silica gel 60 Å with fluorescent indicator (partisil K6F). Compounds were visualized by UV light and/or stained with iodine or potassium permanganate solution with the aid of heat. Flash column chromatography was performed on Whatman silica gel 60 Å (230−400 mesh). NMR (^{1}H and ^{13}C) spectra were recorded on a Varian or Bruker 400 MHz spectrometer and calibrated using an internal reference. ESI mode mass spectra were recorded on a Agilent MSD SL ion trap or Bruker BiotofII mass spectrometer. All the compounds synthesized were racemic mixtures. Purity of the compounds was analyzed by HPLC using 75:25 ACN/H2O as the mobile phase with a flow rate of 0.9 mL/min on a C18 column. All compounds exhibited greater than 95% purity and were tested as racemic mixtures. Intermediate and final compounds were prepared by Nicholas Bleeker (NB), Dr. Balasubramanian Srinivasan (BS), or Dr. Aridoss Gopalakrishnan (AG) as indicated.

2.4.2. Procedure for the synthesis of 2-Hydroxy-5-(3',5'-dimethoxyphenyl)benzaldehyde

5-Bromosalicylaldehyde (1 mmol), (3,5-dimethoxyphenyl)boronic acid (1.2 mmol), palladium(II) acetate (0.05 mmol), potassium carbonate (3 mmol), and triphenylphosphine (0.05 mmol) were taken in 4 mL of DMF/H2O (1:1) mixture and degassed well with nitrogen. The mixture was then heated to 60 °C under N_2 atmosphere

for 16 h. The crude mixture was diluted with water and extracted with ethyl acetate (25 mL × 3) and washed with brine. The combined organic phase was dried over Na_2SO_4 followed by solvent evaporation, which gave a crude product which was further purified by column chromatography to yield the pure product.

2.4.2.1. 2-Hydroxy-5-(3',5'-dimethoxyphenyl)benzaldehyde (NB). Yield: 45%. ^{1}H NMR ($CDCl_3$): δ 11.01 (1H, s, OH), 9.98 (1H, s, CHO), 7.77-7.74 (2H, m, Ar), 7.08 (1H, d, J = 9.0 Hz, Ar), 6.67 (2H, d, J = 3.0 Hz, 2', 6'-H), 6.48-6.46 (1H, m, 4'-H), 3.86 (6H, s, 3',5'-OCH_3). ^{13}C NMR (100 MHz, $CDCl_3$): δ 196.63, 161.27 161.15, 135.74, 133.23, 131.91, 120.62, 118.05, 105.01, 99.14, 55.45.

2.4.3. General procedure for the synthesis of substituted coumarin

To *N*,*N*-dimethylacetamide (1.98 mmol) stirred at 0 °C, phosphorus oxychloride (1.98 mmol) was added dropwise. The reaction mixture was allowed to stir at 0 °C for 30 min followed by addition of the corresponding salicylaldehyde (0.99 mmol) in dry DCM. The reaction solution was then refluxed (at 60 °C) for 4 h. After the allotted duration, the reaction was cooled to room temperature and saturated $NaHCO_3$ solution (10 mL) was added. The combined mixture was heated again to 60 °C for an additional 1 h, cooled, and acidified (1 N HCl). Following extraction with methylene chloride, the combined extracts were dried (anhydrous $MgSO_4$) and concentrated under reduced pressure to afford a crude product, which upon base treatment (NaOH) followed by recrystallization gave the pure compound. If required, purification was carried out by column chromatography.

2.4.3.1. 6-(3',5'-Dimethoxyphenyl)-2*H*-chromen-2-one (NB). Yield: 53%. ^{1}H NMR ($CDCl_3$): δ 7.77-7.65 (3H, m, Ar), 7.41 (1H, d, J = 9.0 Hz, 8-H), 6.69 (2H, m, Ar), 6.49 (2H, m), 3.85 (6H, s, 3',5'-OCH_3). ^{13}C NMR (75 MHz, $CDCl_3$): δ 161.26, 160.65, 155.49, 153.57, 143.42, 141.56, 137.77, 130.76, 126.11, 118.96, 117.21, 117.07, 105.47, 99.48, 55.47.

2.4.4. General procedure for the synthesis of 6-aryl coumarin

6-Bromocoumarin (1 mmol), K_2CO_3 (2.5 mmol), and the respective boronic acid (1.2 mmol) were taken in toluene/water (5:1) (15 mL) and degassed well with nitrogen. To this, $Pd(PPh_3)_4$ (0.05 mol %) was added, and the mixture was stirred at 80 °C under nitrogen atmosphere for 16 h. It was then cooled to 0 °C, acidified with 1N HCl, extracted with ethyl acetate (25 mL × 3), washed with water and brine, and finally dried over $MgSO_4$. Removal of solvent under reduced pressure gave the crude product which upon purification by column chromatography yielded the desired 6-aryl-substituted coumarin.

2.4.4.1. 6-(3-Nitrophenyl)-2*H*-chromen-2-one (AG). Yield: 61%. ^{1}H NMR (400 MHz, $CDCl_3$): δ 8.46 (1H, t, J = 2.0 Hz), 8.26−8.24 (1H, m), 7.93−7.91 (1H, m), 7.81−7.74 (3H, m), 7.66 (1H, t, J = 8.0 Hz), 7.47 (1H, d, J = 8.8 Hz), 6.52 (1H, d, J = 9.6 Hz). ^{13}C NMR (100 MHz, $CDCl_3$): δ 160.40, 154.29, 148.98, 143.18, 141.21, 135.36, 133.03, 130.71, 130.22, 126.49, 122.69, 122.04, 119.49, 117.97, 117.81.

2.4.4.2. 6-(4-Nitrophenyl)-2*H*-chromen-2-one (AG). Yield: 58%. ^{1}H NMR (400 MHz, $CDCl_3$): δ 8.34 (2H, d, J = 8.8 Hz), 7.81−7.73 (5H, m), 7.47 (1H, d, J = 8.4 Hz),

6.52 (1H, d, J = 9.6 Hz). ^{13}C NMR (100 MHz, $CDCl_3$): δ 160.37, 154.48, 147.52, 145.83, 143.19, 135.45, 130.89, 127.93, 126.74, 124.48, 119.47, 117.95, 117.79.

2.4.5. General procedure for reduction of aryl nitro to aryl amine

To a stirred suspension of the respective nitrocoumarin (5 mmol) in methanol (20 mL), 10% Pd/C (0.4 g) was added followed by dry ammonium formate (25−30 mmol). The contents were stirred vigorously under nitrogen at room temperature. Upon completion of reaction, the catalyst was removed by filtration through a bed of Celite and solvent was evaporated under reduced pressure. The resulting crude mass was extracted with ethyl acetate, washed with water, and dried (over $MgSO_4$). Again, solvent was removed under reduced pressure. The resultant solid was purified by column chromatography to isolate the desired amino derivative.

2.4.5.1. 6-(3-Aminophenyl)-2*H*-chromen-2-one (AG). Yield: 65%. ^{1}H NMR (400 MHz, $CDCl_3$): δ 7.76−7.71 (2H, m), 7.63 (1H, d, J = 2.4 Hz), 7.38 (1H, d, J = 8.4 Hz), 7.26−7.23 (1H, m), 6.96 (1H, d, J = 8.0 Hz), 6.88 (1H, t, J = 1.8 Hz), 6.71 (1H, dd, J = 1.6, 8.0 Hz), 6.46 (1H, d, J = 9.2 Hz), 3.79 (2H, s). ^{13}C NMR (100 MHz, $CDCl_3$): δ 160.90, 153.51, 147.13, 143.67, 140.71, 138.18, 130.86, 130.10, 126.12, 119.06, 117.54, 117.25, 117.08, 114.64, 113.73.

2.4.5.2. 6-(4-Aminophenyl)-2*H*-chromen-2-one (AG). Yield: 72%. ^{1}H NMR (400 MHz, $CDCl_3$): δ 7.74 (1H, d, J = 9.6 Hz), 7.68 (1H, dd, J = 2, 8.8 Hz), 7.58 (1H, d, J = 2 Hz), 7.39 (2H, d, J = 8.4 Hz), 7.35 (1H, d, J = 8.4 Hz), 6.77 (2H, d, J = 8.4 Hz), 6.44 (1H, d, J = 9.6 Hz), 3.79 (2H, s). ^{13}C NMR (100 MHz, $CDCl_3$): δ 161.05, 152.92, 146.47, 143.76, 138.01, 130.24, 129.69, 128.08, 125.16, 119.13, 117.24, 116.96, 115.59.

2.4.6. General procedure for the synthesis of substituted alkyl-4*H*-chromene-3-carboxylate

Freshly cut sodium (0.096 mmol) was added to the respective dry alcohol (5 mL), followed by the addition of methyl (for CXL093) or ethyl cyanoacetate (0.192 mmol). The reaction mixture was stirred at room temperature under an inert atmosphere for 30 min, followed by the addition of a solution of the corresponding coumarin (0.08 mmol) in anhydrous alcohol or DCM (3 mL). The resulting reaction mixture was stirred at room temperature. Upon consumption of the coumarin, the reaction mass was concentrated, diluted with water (30 mL), and extracted using ethyl acetate (3 × 20 mL). The organics were combined, washed with water, brine, and dried ($MgSO_4$). Removal of solvent under reduced pressure afforded the crude mass which upon column purification gave the pure product. Note: propargyl alcohol used for this reaction must be rigorously dried.

2.4.6.1 Methyl 2-Amino-6-(3,5-dimethoxyphenyl)-4-(2-methoxy-2-oxoethyl)-4*H*-chromene-3-carboxylate (CXL093, NB). Yield: 35%. ^{1}H NMR (400 MHz, $CDCl_3$): δ 7.45 (1H, d, J = 2.20 Hz), 7.41 (1H, dd, J = 2.25, 8.31 Hz), 7.03 (1H, d, J = 8.30 Hz), 6.67 (2H, d, J = 2.35 Hz), 6.46 (1H, t, J = 2.15 Hz), 6.35 (2H, br. s), 4.35 (1H, dd, J = 4.70, 7.24 Hz), 3.85 (6H, s), 3.78 (3H, s), 3.59 (3H, s), 2.69 (1H, dd, J = 4.70, 14.80 Hz), 2.62 (1H, dd, J = 7.20, 14.80 Hz). ^{13}C NMR (100 MHz, CDCl3): δ 172.0, 169.4, 161.6, 161.1, 142.5, 137.5, 127.0, 126.5, 125.8, 116.1, 105.2, 105.0, 99.2, 76.5, 55.4, 51.4, 51.0, 43.5, 31.4. MS (ESI, positive) m/z calcd for $C_{22}H_{24}NO_7$ $(M + H)^+$: 414.16; found: 414.21.

.**2.4.6.2. Propyl 2-Amino-6-(3,5-dimethoxyphenyl)-4-(2-oxo-2-propoxyethyl)-4*H*-chromene-3-carboxylate (CXL041, NB).** Yield: 58%. ^{1}H NMR (400 MHz, $CDCl_3$): δ 7.45 (1H, d, J = 2.26 Hz), 7.40 (1H, dd, J = 2.13, 8.41 Hz), 7.02 (1H, d, J = 8.28 Hz), 6.67 (2H, d, J = 2.26 Hz), 6.46 (1H, t, J = 2.26 Hz), 6.34 (2H, br. s), 4.37 (1H, dd, J = 4.02, 7.78 Hz), 4.15 (2H, t, J = 6.65 Hz), 3.94 (2H, dt, J = 2.38, 6.71 Hz), 3.85 (6H, s), 2.75-2.58 (2H, m), 1.75 (2H, sxt, J = 7.08 Hz), 1.53 (2H, qd, J = 7.19, 14.31 Hz), 1.03 (3H, t, J = 7.40 Hz), 0.81 (3H, t, J = 7.40 Hz). ^{13}C NMR (100 MHz, $CDCl_3$): δ 171.74, 169.10, 161.43, 161.05, 149.56, 142.53, 137.44, 127.05, 126.45, 125.79, 116.08, 105.19, 99.21, 65.89, 65.25, 55.40, 43.67, 31.42, 29.69, 22.31, 21.84, 10.66, 10.28. MS (ESI, positive) m/z calcd for $C_{26}H_{31}NO_7$ $(M + H)^+$: 470.22; found: 470.20.

2.4.6.3. Butyl 2-Amino-4-(2-butoxy-2-oxoethyl)-6-(3,5-dimethoxyphenyl)-4*H*-chromene-3-carboxylate (CXL042, NB). Yield: 63%. ^{1}H NMR (400 MHz, $CDCl_3$): δ 7.45 (1H, d, J = 2.26 Hz), 7.40 (1H, dd, J = 2.26, 8.28 Hz), 7.02 (1H, d, J = 8.28 Hz), 6.68 (2H, d, J = 2.26 Hz), 6.46 (1H, t, J = 2.26Hz), 6.34 (2H, br. s), 4.35 (1H, dd, J = 4.02, 7.53 Hz), 4.19 (2H, t, J = 6.15Hz), 3.98 (2H, t, J = 7.53Hz), 3.85 (6H, s), 2.74-2.56 (2H, m), 1.76-1.65 (2H, m), 1.55-1.41 (4H, m), 1.24 (2H, qd, J = 7.38, 15.00 Hz), 0.98 (3H, t, J = 7.40 Hz), 0.84 (3H, t, J = 7.40 Hz). ^{13}C NMR (100 MHz, $CDCl_3$): δ 171.74, 169.10, 161.41, 161.04, 149.53, 142.50, 137.42, 127.05, 126.43, 125.76, 116.06, 105.19, 99.17, 64.18, 63.45, 55.38, 43.66, 31.39, 31.01, 30.53, 19.33, 19.03, 13.78, 13.62. MS (ESI, positive) m/z calcd for $C_{28}H_{35}NO_7$ $(M + H)^+$: 498.25; found: 498.21.

2.4.6.4. Allyl 4-(2-(Allyloxy)-2-oxoethyl)-2-amino-6-(3,5-dimethoxyphenyl)-4*H*-chromene-3-carboxylate (CXL043, NB). Yield: 47%. ^{1}H NMR (400 MHz, $CDCl_3$): δ 7.46 (1H, d, J = 2.01 Hz), 7.40 (1H, dd, J = 2.13, 8.41 Hz), 7.02 (1H, d, J = 8.53 Hz), 6.67 (2H, d, J = 2.26 Hz), 6.46 (1H, t, J = 2.13 Hz), 6.38 (2H, br s), 5.95-6.08 (1H, m), 5.73-5.85 (1H, m), 5.39 (1H, d, J = 17.32 Hz), 5.07-5.28 (3H, m), 4.70 (2H, d, J = 5.27 Hz), 4.48 (2H, d, J = 5.77 Hz), 4.41 (1H, dd, J = 4.27, 7.28 Hz), 3.85 (6H, s), 2.62-2.79 (2H, m). ^{13}C NMR (101 MHz, $CDCl_3$): δ 171.23, 168.54, 161.75, 161.05, 149.53, 142.44, 137.54, 133.00, 132.02, 127.06, 126.52, 125.66, 118.18, 117.18, 116.11, 105.21, 99.21, 65.01, 64.25, 55.39, 43.58, 31.35. MS (ESI, positive) m/z calcd for $C_{26}H_{27}NO_7$ $(M + H)^+$: 466.19; found: 466.21.

2.4.6.5. Cyclopropylmethyl 2-Amino-4-(2-(cyclopropylmethoxy)-2-oxoethyl)-6-(3,5-dimethoxyphenyl)-4*H*-chromene-3-carboxylate (CXL046, NB). Yield: 46%. ^{1}H NMR (400 MHz, $CDCl_3$): δ 7.48 (1H, d, J = 2.26 Hz), 7.40 (1H, dd, J = 2.26, 8.28 Hz), 7.02 (1H, d, J = 8.53 Hz), 6.67 (2H, d, J = 2.26Hz), 6.45 (1H, t, J = 2.26Hz), 6.42-6.00 (2H, br. s), 4.40 (1H, dd, J = 4.27, 7.28 Hz), 4.08-3.98 (2H, m), 3.85 (6H, s), 3.80 (2H, dd, J = 1.25, 7.28 Hz), 2.79-2.65 (2H, m), 1.27 (2H, s), 0.62-0.56 (2H, m), 0.48-0.42 (2H, m), 0.37-0.31 (2H, m), 0.18-0.13 (2H, m). ^{13}C NMR (100 MHz, $CDCl_3$): δ 170.8, 168.1, 160.4, 160.0, 148.6, 141.5, 136.4, 126.1, 125.4, 124.8, 115.1, 104.2, 98.2, 76.3, 76.0, 75.7, 68.0, 67.1, 54.4, 42.5, 30.4, 28.7, 9.1, 8.7, 2.2, 2.1, 2.1, 2.1. MS (ESI, positive) m/z calcd for $C_{28}H_{31}NO_7$ $(M +H)^+$: 494.22; found: 494.40.

2.4.6.6. Prop-2-yn-1-yl 2-Amino-6-(3,5-dimethoxyphenyl)-4-(2-oxo-2-(prop-2-yn-1-yloxy)ethyl)-4*H*-chromene-3-carboxylate (CXL035, BS). Yield: 43%. ^{1}H NMR (400 MHz, $CDCl_3$): δ 7.46 (1H, d, J = 2.0 Hz), 7.40 (1H, dd, J = 2.0 Hz, 8.4 Hz), 7.02 (1H, d, J = 8.4 Hz), 6.66 (2H, d, J = 2.0 Hz), 6.44 (1H, t, J = 2.0 Hz), 6.39 (2H, br. s), 4.79-4.78 (2H, m), 4.64-4.54 (2H, m), 4.39 (1H, dd, J = 4.8 Hz, 8.4 Hz), 3.84 (6H, s), 2.77-2.66 (2H, m), 2.47 (3H, t, J = 2.4 Hz), 2.31 (3H, t, J = 2.4 Hz). ^{13}C NMR (75 MHz, $CDCl_3$): δ 170.64, 167.88, 162.20, 161.05, 149.45, 142.40, 137.78, 127.09, 126.70, 125.39, 116.19, 105.31, 99.24, 78.68, 75.86, 74.89, 74.28, 55.43, 51.81, 51.16, 43.33, 31.12. MS (ESI, positive) m/z calcd for $C_{26}H_{23}NO_7$ $(M+Na)^+$: 484.15; found: 484.46.

2.4.6.7. Prop-2-yn-1-yl 2-Amino-6-(3-aminophenyl)-4-(2-oxo-2-(prop-2-yn-1-yloxy)ethyl)-4*H*-chromene-3-carboxylate (CXL055, AG). Yield: 59%. ^{1}H NMR (400 MHz, $CDCl_3$): δ 7.45 (1H, d, J = 2 Hz), 7.38 (1H, dd, J = 2, 8.4 Hz), 7.19 (1H, t, J = 8.0 Hz), 7.01 (1H, d, J = 8.4 Hz), 6.92 (1H, d, J = 7.6 Hz), 6.85 (1H, t, J = 2 Hz), 6.66 (1H, dd, J = 1.6, 8.0 Hz), 6.41 (2H, s), 4.79 (2H, t, J = 2.2 Hz), 4.60−4.59 (2H, m), 4.41−4.38 (1H, m), 3.74 (2H, s), 2.78−2.64 (2H, m), 2.47 (1H, t, J = 2.0 Hz), 2.29 (1H, t, J = 2.6 Hz). ^{13}C NMR (100 MHz, $CDCl_3$): δ 170.81, 167.97, 162.35, 149.26, 146.85, 141.41, 138.02, 129.75, 127.02, 126.63, 125.33, 117.45, 116.18, 114.11, 113.75, 78.83, 77.71, 75.89, 75.04, 74.41, 51.89, 51.21, 43.47, 31.23. MS (ESI, positive) m/z calcd for $C_{24}H_{20}N_2O_5$ $(M + H)^+$: 417.14; found: 417.1.

2.4.6.8. Prop-2-yn-1-yl 2-Amino-6-(4-aminophenyl)-4-(2-oxo-2-(prop-2-yn-1-yloxy)ethyl)-4*H*-chromene-3-carboxylate (CXL070, AG). Yield: 67%. ^{1}H NMR (400 MHz, $CDCl_3$): δ 7.41 (1H, d, J = 1.8 Hz), 7.35 (3H, d, J = 8.4 Hz), 7.00 (1H, d, J = 8.4 Hz), 6.73 (2H, d, J = 8.4 Hz), 6.39 (2H, s), 4.35−4.79 (2H, t, J = 2 Hz), 4.58 (2H, t, J = 2.4 Hz), 4.39−4.37 (1H, m), 3.72 (2H, s), 2.77−2.65 (2H, m), 2.47 (1H, t, J = 2 Hz), 2.28 (1H, t, J = 2.2 Hz). ^{13}C NMR (100 MHz, $CDCl_3$): δ 170.88, 168.07, 162.47, 148.68, 145.95, 137.97, 130.71, 127.98, 126.27, 125.97, 125.39, 116.23, 115.47, 78.87, 77.77, 76.06, 74.97, 74.37, 51.92, 51.25, 43.53, 31.32. MS (ESI, positive) m/z calcd for $C_{24}H_{20}N_2O_5$ $(M + H)^+$: 417.14; found: 417.2.

2.4.7. Procedure for the epoxidation of CXL043 to give CXL086

To a stirred solution of CXL043 (0.17 mmol) in dry DCM under nitrogen at 0 °C was added 0.37 mmol of *m*-CPBA over a period of 5 min. After 1 h, the ice bath was removed and the mixture was left to reach room temperature over 24 h. The reaction mixture was extracted with sodium bicarbonate, washed with brine, dried over Na_2SO4, filtered, and concentrated in vacuo. The residue was purified by column chromatography to afford the pure compound.

2.4.7.1. Oxiran-2-ylmethyl 2-Amino-6-(3,5-dimethoxyphenyl)-4-(2-(oxiran-2-ylmethoxy)-2-oxoethyl)-4*H*-chromene-3-carboxylate (CXL086, NB). Yield: 48%. ^{1}H NMR (400 MHz, $CDCl_3$): δ 7.52 (1H, dd, J = 2.25, 8.51 Hz), 7.40 (1H, d, J = 2.15 Hz), 7.29 (1H, d, J = 8.41 Hz), 6.64 (2H, d, J = 2.15 Hz), 6.48 (1H, t, J = 2.15 Hz), 5.76−5.95 (1H, m), 5.23−5.34 (2H, m), 5.19−5.26 (2H, m), 5.12 (2H, dd, J = 4.60, 9.88 Hz), 5.04 (2H, br. s), 4.64 (2H, tt, J = 1.20 Hz, 5.84 Hz), 4.59 (2H, tt, J = 1.20 Hz, 5.80 Hz), 3.85

(6H, s), 3.29 (1H, dd, J = 9.98, 17.22 Hz), 2.74 (1H, dd, J = 4.50, 17.22 Hz). ^{13}C NMR (100 MHz, $CDCl_3$): δ 191.4, 171.1, 161.1, 160.0, 154.0, 148.1, 141.9, 139.6, 131.8, 130.6, 128.5, 128.0, 123.6, 119.7, 118.5, 105.5, 99.5, 66.9, 65.7, 55.4, 45.0, 35.8 (two coinciding carbon resonances). MS (ESI, positive) m/z calcd for $C_{26}H_{27}NO_9$ $(M + H)^+$: 498.18; found: 498.16.

2.4.8. Cell cultures

HL60, HL60/MX2, CCRF-CEM, and CCRF-CEM/C2 were purchased from ATCC. HL60/MX2 was developed from HL60 upon exposure to mitoxantrone, a topoisomerase II inhibitor. CCRF-CEM/C2 was developed from CCRF-CEM upon exposure to camptothecin, a topoisomerase I inhibitor. K562, K562/HHT300, K562/DOX, HL60/ADR, and HL60/DNR cell lines were provided by Dr. Tang.[118] K562/HHT300 was developed from K562 upon exposure to homoharringtonine, an antimicrotubule agent. K562/DOX was developed from K562 upon exposure to doxorubicin, a topoisomerase II inhibitor. HL60/ADR and HL60/DNR were developed from HL60 upon exposure to adriamycin (a.k.a. doxorubicin) and daunorubicin, respectively. Both adriamycin and daunorubicin are topoisomerase II inhibitors. HL60 and HL60/DOX cell lines were provided by Dr.Ganapathi.[111] HL60/DOX was developed from HL60 upon exposure to doxorubicin. CCRF-CEM, CCRF-CEM/VM-1-5, and CCRF-CEM/VLB100 were provided by Dr. Beck.[116,117] CCRF-CEM/VM-1-5 was developed from CCRF-CEM upon exposure to teniposide, a topoisomerase II inhibitor. CCRF-CEM/VLB100 was developed from CCRF-CEM upon exposure to vinblastine, an antimicrotubule agent. As HL60/ADR and HL60/DOX are from two different sources,

they do not possess an equivalent therapeutic response. Similarly the three parental HL60 cell lines and the two parental CCRF-CEM cell lines exhibit different sensitivities to the same therapy. Therefore, all cell lines were given the designation provided in their original literature reports. Comparison has been made only between the MDR cell lines and their corresponding parental cell lines. Lastly, all cell lines were grown in RPMI 1640 media (ATCC) supplemented with 10% FBS and incubated at 37 °C under 5% CO_2 in air.

2.4.9. Cell viability measurement

Cytotoxicity was assessed via a growth inhibition assay as reported previously.[105] Cells were plated in 96-well plates at $1x10^4$ cells/well and treated with serial dilutions of each compound in the presence of 1% DMSO. Following 48-hour incubation, relative cell viability was determined using the CellTiter-Blue cell viability assay kit (Promega, Madison, WI). Data were plotted (relative cell viability vs. log[drug]) and fit using GraphPad Prism (San Diego, CA) according to a four-parameter dose-response equation (Equation 2.1). Based on the fit, the IC_{50} of each compound was determined.

$$\boldsymbol{Y = Y_{min} + \frac{(Y_{max} - Y_{min})}{1 + 10^{n(pIC_{50} - p[X])}}}$$

Equation 2.1. Four-parameter dose-response equation

CHAPTER 3*

Multidrug-Resistant AML is Susceptible to SERCA Inhibitors

3.1. Introduction

Structure-activity relationship studies of sHA 14-1, a dual inhibitor against Bcl-2 and SERCA, led to the discovery of ethyl 2-amino-6-(3,5-dimethoxyphenyl)-4-(2-ethoxy-2-oxoethyl)-4*H*-chromene-3-carboxylate, CXL017, an improved lead for the treatment of multidrug-resistant leukemia.[108] Previous work indicated that sHA 14-1 targets both ER and mitochondrial dynamics in order to elicit its cytotoxic effect. In particular, sHA 14-1 was shown to inhibit the ER Ca^{2+}-ATPase, SERCA as well as manipulate Bcl-2 family proteins.[106] The ability of CXL017 to mitigate multidrug-resistant cancer and its structural similarity with sHA 14-1 provide impetus for better understanding the inhibition of SERCA by CXLs in order to relate disrupted calcium mobilization to the targeting of multidrug-resistant leukemia.

Given that CXL017 is one of the most potent members of the CXL series in cell a viability measurement, this compound was selected for initial screening against the calcium pump. Accordingly, CXL017 was found to have no effect on the calcium affinity of SERCA, compete with ATP, and cause a dose-responsive decrease in SERCA ATPase activity. Among the six CXLs evaluated (Figure 3.1), (-)-CXL017 proved to be most potent SERCA inhibitor. Inhibitor combination studies revealed strong synergy between (-)-CXL017 and three well-known SERCA inhibitors: TG, CPA, and BHQ (Figure 1.8). However, no combinations of the known inhibitors proved to be

* Parts of this chapter have been reproduced with permission from Bleeker, N. P. *et al*. A novel SERCA inhibitor demonstrates synergy with classic SERCA inhibitors and targets multidrug-resistant AML. *Mol. Pharmaceutics*, In press. Unpublished work © 2013 American Chemical Society.

synergistic. In cytotoxicity experiments in HL60 and HL60/MX2 cells, both CXLs and the known SERCA inhibitors demonstrated selectivity for the resistant line. In addition, the combination of (-)-CXL017 and TG yielded synergistic cytotoxicity in HL60/MX2 cells. Analysis of SERCA inhibition and cytotoxicity in HL60/MX2 revealed a positive correlation that was not observed in HL60. Together these results support the proposal that SERCA is indeed the target of CXLs in HL60/MX2, and that the resulting inhibition contributes to the unique ability of these compounds to target this resistant AML cell line.

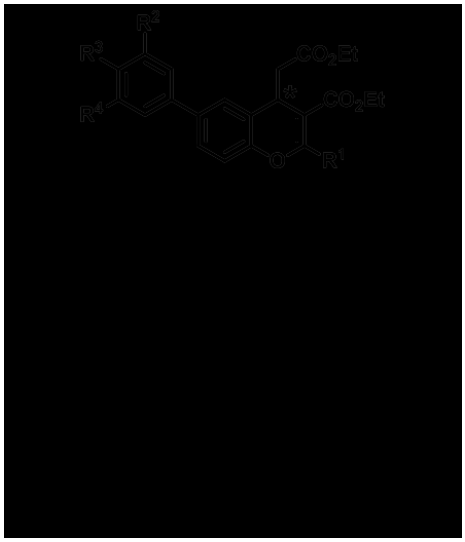

Figure 3.1. Chemical structures of CXL small molecules used in chapter 3. Asterisk (*) denotes a chiral center.

3.2. Results and Discussion

3.2.1. Characterization of CXL017 as an inhibitor of SERCA

The catalytic mechanism of SERCA allows two Ca^{2+} ions to be translocated across the ER membrane per molecule of ATP hydrolyzed.[121] This pumping action is facilitated by the movement of three cytoplasmic domains (A, actuator; P,

phosphorylation; and N, nucleotide binding) in concert with 10 transmembrane helices. During the multi-step enzymatic cycle, ATP binds within the N domain leading to phosphorylation within the P domain and the ultimate translation of movement to afford the necessary conformational adjustments that result in active Ca^{2+} transport into the ER.[122] Presumably, an inhibitor could disrupt the enzymatic action of SERCA by interfering with Ca^{2+} binding, ATP binding, or both. To test the potential effects of CXL017 on Ca^{2+} and ATP utilization, each substrate was varied (while the other was held constant) in the ATPase assay and CXL017 was introduced at either 10 or 30 μM. First, free Ca^{2+} was varied from pCa 5 to 7 and the resulting data set was fitted to the Hill equation to obtain normalized V_{max} and pK_{Ca} values. While CXL017 displayed no significant effect on the apparent Ca^{2+} affinity (pK_{Ca}) of SERCA, a dose-dependent decrease in V_{max} was observed (Fig. 3.2A and C) with a normalized V_{max} of 0.80 ± 0.04 and 0.40 ± 0.01 in the presence of 10 μM and 30 μM CXL017 respectively.

Effects on ATP utilization were measured in a similar manner, with pATP ranging from 2.6 to 6.4. In this case, the data were fitted to a bi-Michaelis Menten equation to accommodate two ATP binding sites; the first, a higher affinity catalytic site and the second, a lower affinity regulatory site.[123] The V_{max} at both the catalytic and regulatory sites was well-defined by the two-site model in the absence of inhibitor and yielded no significant change in the presence of 10 or 30 μM CXL017 (data not shown). Since changes in $V_{max(reg)}$ and $V_{max(cat)}$ were not detected, data was reprocessed with the value for the catalytic and regulatory V_{max} fixed to the values obtained in the control experiment (Figure 3.2.B, circles), which provided equally good fits of the data ($r^2 \geq$

0.99). With these constraints, CXL017 showed apparent competition with ATP at both the high and low affinity sites in comparison to control ($pK_{ATP(cat)}$ = 4.99 ± 0.07 and $pK_{ATP(reg)}$ =3.30 ± 0.08). Specifically, $pK_{ATP(cat)}$ was 3.92 ± 0.02 and $pK_{ATP(reg)}$ was 2.96 ± 0.07 in the presence of 10 μM CXL017, and $pK_{ATP(cat)}$ was 3.99 ± 0.02 and $pK_{ATP(reg)}$ was 2.6 ± 0.1 in the presence of 30 μM CXL017 (Figure 3.2B and D). Thus, the reduction of pK_{ATP} at the regulatory site responded in a dose-responsive manner, whereas the catalytic site was similarly affected by 10 and 30 μM CXL017.

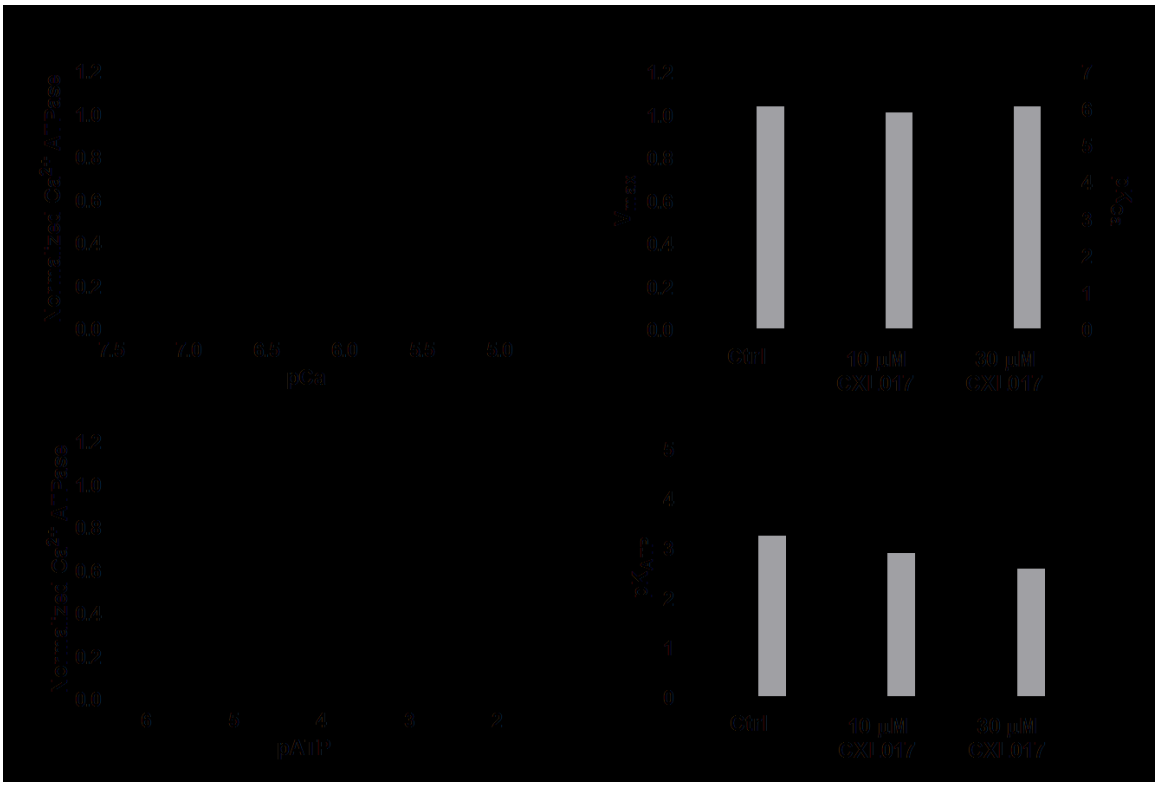

Figure 3.2. Characterization of SERCA inhibition by CXL017. (A) Ca^{2+}-ATPase activity, normalized to V_{max} of control, measured with varied [Ca^{2+}] (pCa 7.5-5.0) and fixed [ATP] (pATP = 2.6), in the presence of no inhibitor (●), 10 μM CXL017 (■), and 30 μM CXL017 (▲). Curves show fits to the Hill equation (Eq. 1). (B) Ca^{2+}-ATPase

activity measured with varied [ATP] (pATP 6.2-2.6) and fixed [Ca^{2+}] (pCa = 5.4) in the presence of no inhibitor (●), 10 μM CXL017 (■), and 30 μM CXL017 (▲). Curves show fits to the Bi-Michaelis Menten equation (Eq. 2). (C) Effect on V_{max} (black, left y-axis) and pK_{Ca} (gray, right y-axis) by 10 and 30 μM CXL017 as determined from a fit in A. (D) Effect on p$K_{ATP(cat)}$ (black) and p$K_{ATP(reg)}$ (gray) by 10 and 30 μM CXL017 as determined from fits in B. Data are expressed as mean ± SEM, n = 3. Figures are representative of three independent experiments.

The kinetic data relating to SERCA activity in the presence of varied calcium or ATP provide insight into the mode of inhibition by CXL017. Though the apparent calcium affinity (K_{Ca}) of the enzyme is not affected by CXL017, V_{max} for ATPase activity at saturating calcium decreases in a dose-dependent manner (Fig. 2A and C). Furthermore, CXL017 competes with ATP, as indicated by the rightward shift in Fig. 2C, and demonstrates differential inhibition at the regulatory and catalytic binding sites, leading to a dose-dependent response exclusively at the regulatory site (Fig. 2D). Since the physiological range of ATP is in the range of 2-10 mM (pATP ≤ 2.7), the regulatory site is probably more relevant to SERCA inhibition in cells.[124] Although the competition observed at the regulatory site may be due to CXL017 occupying the nucleotide-binding domain directly, conformational changes within SERCA are often transmitted allosterically throughout the length of the protein, such that even binding in the TM domain can elicit effects on the flexibility of the cytoplasmic domains.[125] For example, TG and CPA are both known to bind in the TM domain, but each induces unique changes

to the cytoplasmic headpiece.[95] Thus, further experimentation is needed to determine the binding site of CXL017 within the ER Ca^{2+}-ATPase.

3.2.2. Investigation of CXLs as SERCA inhibitors

In order to compare the potency of CXL017 with other members of the CXL series, 5 other CXLs were selected and evaluated alongside CXL017 in the ATPase assay with the concentration of substrates held constant to maximize SERCA activity and assay sensitivity. CXLs demonstrated only partial SERCA inhibition with the most potent inhibitor providing a saturating amount of inhibition near 50%. A fit of the data (Equation 2.1) was implemented to determine the IC_{50} of each inhibitor (Figure 3.3). As predicted, based on the cytotoxicity of these inhibitors, CXL017 was the most potent among the racemic compounds evaluated with an IC_{50} of 25 ± 1 μM. In addition, (-)-CXL017 (IC_{50} = 13.5 ± 0.5 μM) proved to be nearly 5 times more potent than (+)-CXL017 (IC_{50} of 68 ± 11 μM), similar to the eudysmic ratio observed in cell viability experiments and providing evidence that SERCA is the intracellular target of CXLs.[108]

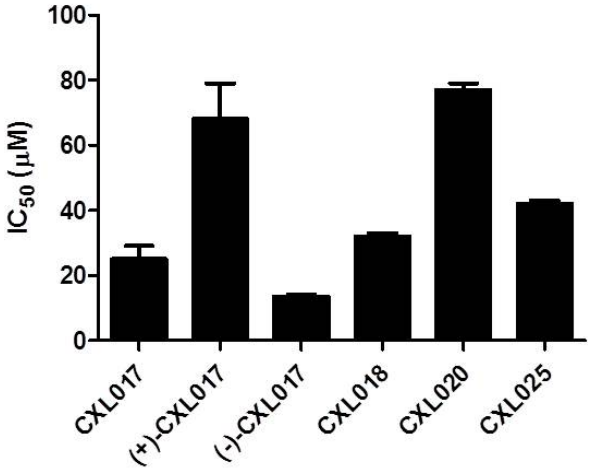

Figure 3.3. Inhibition of SERCA enzyme activity by CXLs. CXL small molecules were introduced into the ATPase assay at various concentrations (0-60 μM) with fixed [Ca^{2+}] and [ATP]. The resulting dose-response curve was fit by a four-parameter dose-response equation (Equation 2.1) to give the IC_{50} value of each inhibitor. Data are expressed as mean ± SEM, n = 3. Figure is representative of three independent experiments.

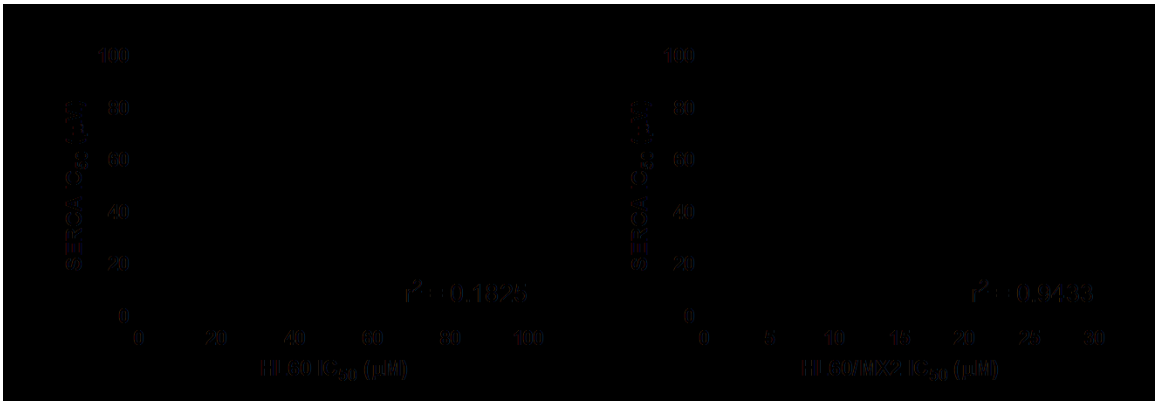

Figure 3.4. Correlation of SERCA inhibition with cytotoxicity in HL60 and HL60/MX2 among CXL compounds. CXL small molecules were evaluated in the SERCA activity assay (described and illustrated in Figure 3.3) and their respective

inhibition was correlated with their respective cytotoxicity in HL60 and HL60/MX2 as previously reported. The r^2 value describes the goodness of fit for the linear regression line. (A) Correlation of SERCA inhibition and cytotoxicity in HL60 cells. (B) Correlation of SERCA inhibition and cytotoxicity in HL60/MX2 cells.

In cytotoxicity experiments, CXL017 was established as a lead for the treatment of multidrug-resistant leukemia.[108] Several analogues have been prepared that reveal a narrow structure-activity relationship within the CXL series.[126] Similarly, five CXLs, evaluated in the SERCA activity assay, demonstrate low- to mid-micromolar inhibitory potencies despite modest changes in chemical structure (Figure 3.3). Two observations are particularly interesting from these experiments. First, the eudysmic ratio observed in cytotoxicity experiments is maintained in SERCA inhibition such that (-)-CXL017 is the eutomer. In fact, (-)-CXL017 is thirteen and tenfold more cytotoxic than (+)-CXL017 in HL60 and HL60/MX2 respectively, while (-)-CXL017 is fivefold more potent than (+)-CXL017 in the SERCA activity assay (Figure 3.3). Secondly, while no correlation exists between SERCA inhibition and the cytotoxicity recorded in HL60 cells, a good correlation exists between the former and the cytotoxicity recorded in HL60/MX2 cells (Figure 3.4 A and B). In light of the elevated SERCA levels and ER calcium content in HL60/MX2 compared to HL60, this correlation strongly suggests that SERCA inhibition is responsible for the collateral sensitivity of HL60/MX2 to CXL small molecules.[109]

3.2.3. (-)-CXL017 synergizes with known SERCA inhibitors

Proving to be the most potent SERCA inhibitor among the CXLs evaluated, (-)-CXL017 was further investigated for potential interaction with three well-known SERCA inhibitors: TG, CPA, and BHQ (see Chapter 1). In this study, the Chou and Talalay method was employed by application of the CompuSyn program, which provides a mechanism-independent method for quantitative determination of drug interactions (calculated as the combination index (CI)), based on the mass-action law.[127] A CI ranging from 0.9 to 1.1 is considered additive, while a CI < 0.9 indicates synergy, and a CI > 1.1 indicates antagonism. Employing this method, the four inhibitors were investigated for synergistic, additive, or antagonistic interaction by introduction into the SERCA activity assay both individually and in combination (6 total combinations) at appropriate fixed molar ratios. Quite surprisingly, (-)-CXL017 demonstrated marked synergy with each of the known SERCA inhibitors (Figure 3.5 A-C), whereas all combinations of the known inhibitors were mostly additive and did not synergize (Figure 3.5 D-F). All combinations that include (-)-CXL017 result in CIs $<<1$, whereas the combinations of TG, CPA, and BHQ gave CIs ≥ 0.9. Among the interactions with (–)-CXL017, BHQ provided the strongest synergy, followed by CPA and TG. These results suggest that (-)-CXL017 binds at a site within SERCA that is distinct from the binding sites of the known inhibitors in order to simultaneously occupy the SERCA structure and provide enhanced combinatorial inhibition.

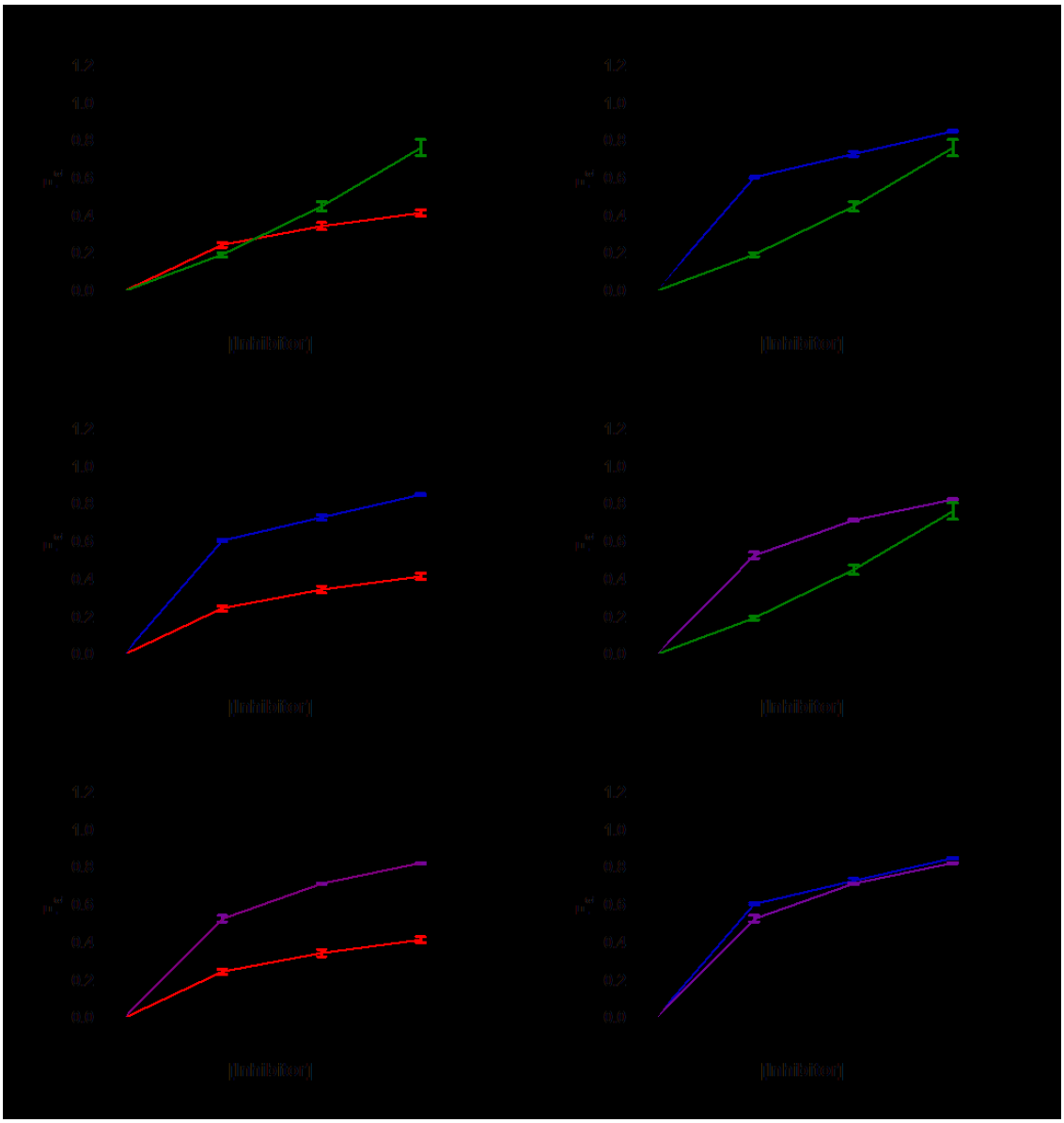

Figure 3.5. Characterization of synergy between (-)-CXL017 and known SERCA inhibitors. (–)-CXL017, TG, CPA, and BHQ were introduced into the ATPase assay at the indicated concentrations both individually (see color indications) and in pairs (—) with fixed [Ca^{2+}] and [ATP]. Inhibitor concentrations were as follows: (-)-CXL017 (—), 6.25 µM, 12.5 µM, and 25 µM; TG (—), 18.75 nM, 37.5 nM, and 75 nM; CPA (—), 0.16 µM, 0.31 µM, and 0.63 µM; BHQ (—), 0.31 µM, 0.63 µM, and 1.25 µM.

(A) (-)-CXL017 and TG dosed individually and in combination at a molar ratio of 667:1. (B) (-)-CXL017 and CPA dosed individually and in combination at a molar ratio of 80:1. (C) (-)-CXL017 and BHQ dosed individually and in combination at a molar ratio of 40:1. (D) TG and CPA dose individually and in combination at a molar ratio of 1:8.33. (E) TG and BHQ dose individually and in combination at a molar ratio of 1:16.7. (F) CPA and BHQ dosed individually and in combination at a molar ratio of 1:2. Data for generation of dose-effect (f_a) plots and calculation of the combination indices (indicated above data points) was facilitated by CompuSyn. CI<0.9, CI=0.9-1.1, and CI>1.1 indicate synergy, additive effect, and antagonism, respectively. Data are expressed as mean ± SEM, n = 9 for inidividual inhibitor plots, n = 3 for inhibitor combination plots. Figures are representative of two independent experiments.

3.2.4. SERCA inhibitors selectively target multidrug-resistant leukemia

HL60/MX2 is well-characterized as a non-P-gp mediated multidrug-resistant AML cell line with respect to HL60, the parental AML line.[126] Previously, HL60/MX2 cells demonstrated collateral sensitivity to CXLs, with 2-7 fold selectivity for the resistant line.[108] In addition, HL60/MX2 cells exhibited elevated levels of SERCA2, SERCA3, and ER calcium content relative to HL60 cells.[109] Taken together, these findings suggest the possibility that SERCA inhibition is the primary mechanism for compounds selectively targeting HL60/MX2. To test this hypothesis, the selectivity ratio of each of the known SERCA inhibitors was evaluated in a cell viability assay in both HL60/MX2 and HL60. Remarkably, TG, CPA, and BHQ all demonstrated selectivity for

the resistant cell line (Figure 3.6). TG was the most potent and selective with an IC_{50} of 0.007 ± 0.001 μM in HL60/MX2 and an IC_{50} of 3 ± 1 μM in HL60, giving a selectivity of 400 fold. Though considerably less potent, both CPA and BHQ also provided good selectivity, with values of 17 and 7.7 fold respectively. Since the cytotoxic SERCA inhibitors, including (–)-CXL017, all demonstrate selectivity towards HL60/MX2, SERCA inhibition may provide one strategy for targeting multidrug resistance in cancer chemotherapy.

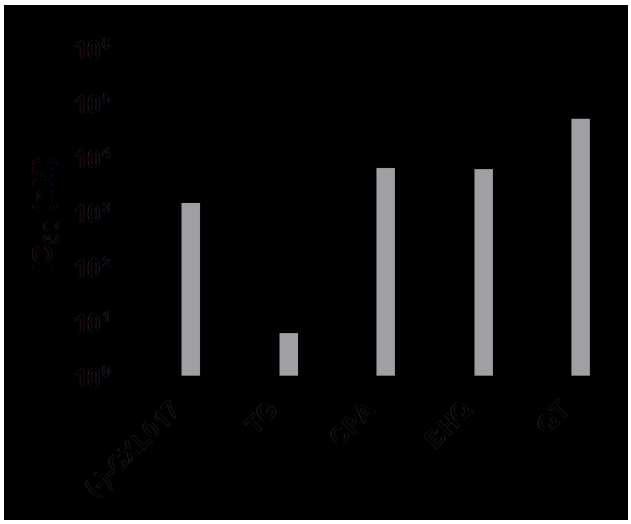

Figure 3.6. Cytotoxicity of SERCA inhibitors in MDR AML. (-)-CXL017, TG, CPA, and BHQ were evaluated in a cell viability assay at various concentrations in HL60 and HL60/MX2 cells. The IC_{50} of each inhibitor in HL60 (black) and HL60/MX2 (gray) was determined by a fit of the respective dose-response curves to the four-parameter dose-response equation (Equation 2.1). Data are expressed as mean ± SEM, n = 3. Figure is representative of three independent experiments.

The scope of SERCA inhibition in overcoming drug resistance across multiple cancer types remains to be determined. However, among nine resistant leukemia cell lines, where a related CXL (CXL070) compound maintained efficacy, TG succumbs to resistance in five of the nine lineages (see Chapter 2).[126] Of the cells displaying resistance to thapsigargin, four are reported to overexpress P-gp, suggesting that TG is subject to drug efflux. Yet this may also suggest that the different binding modes exerted by CXLs and TG are significant with respect to the resultant cellular response. Regardless of the molecular rationale, the utility of CXLs in treating multidrug-resistant leukemia has been demonstrated, and with respect to HL60/MX2, this can likely be attributed to SERCA inhibition. Future experimentation will determine the impact of P-gp on TG resistance and whether SERCA alone is responsible for the cytotoxicity of CXLs across various cancer models.

3.2.5. (-)-CXL017 and thapsigargin synergize in HL60/MX2

Given the impressive synergy observed between (-)-CXL017 and the known SERCA inhibitors, it was hypothesized that this same synergy could be exploited to target HL60/MX2 by combining (-)-CXL017 with one of the other inhibitors in cells. Since it demonstrated the greatest selectivity for HL60/MX2 cells and is one of the most clinically relevant SERCA inhibitors, TG was selected for these experiments. Accordingly, (-)-CXL017 and TG were evaluated as individual inhibitors and in combination at a constant molar ratio; while cell viability was assessed by cell counting based on the uptake of trypan blue. Two concentrations of (-)-CXL017 (12.5 and 6.25

μM) and TG (18.75 nM and 9.375 nM) were evaluated to give four possible inhibitor combinations. Treatment with 6.25 μM (-)-CXL017 and 9.38 nM TG reduced cell viability to 47% and 43% respectively, whereas the combination of the two inhibitors reduced cell viability to 17% (Fig. 6). A similar outcome was observed with the other combinations evaluated. This result is in agreement with the synergism observed in the SERCA activity assay and provides additional support that (-)-CXL017 mediated cytotoxicity in HL60/MX2 is related to SERCA inhibition.

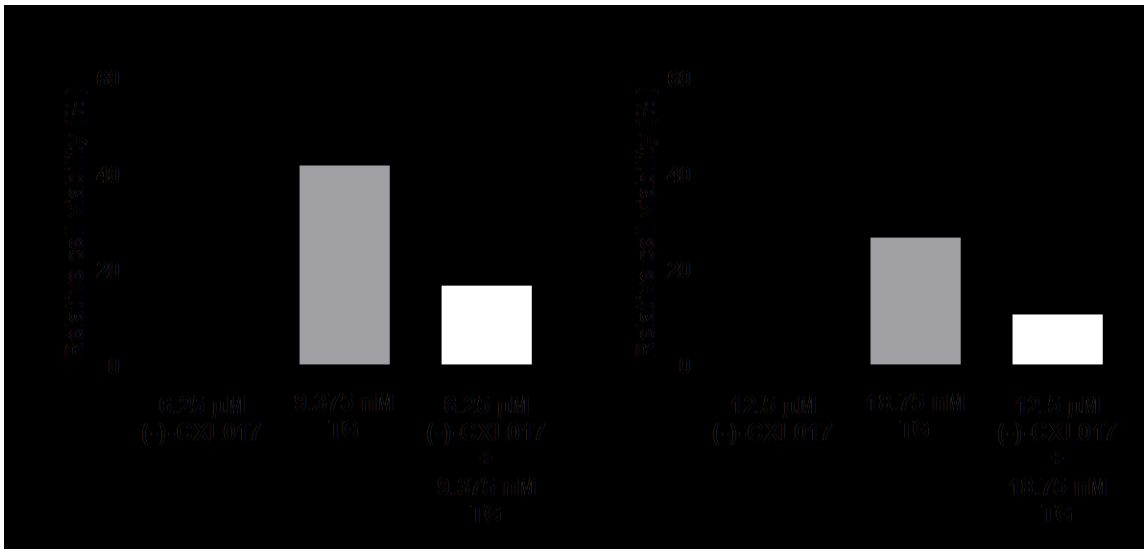

Figure 3.7. Synergy between (-)-CXL017 and TG in HL60/MX2 cells. (-)-CXL017 and TG were evaluated in a cell viability assay individually and in combination at the indicated concentrations to give a molar ratio of 667:1. Relative cell viability was determined based on trypan blue dye exclusion in treated cells. (A) 6.25 μM (-)-CXL017 (black), 9.375 nM TG (gray), and the combination thereof (white). (B) 12.5 μM (-)-CXL017 (black), 18.75 nM TG (gray), and the combination thereof (white). Data are expressed as mean ± SEM, n = 3. Figure is representative of three independent experiments.

Drug combinations have proven to be an invaluable strategy for understanding mechanisms of enzyme inhibition but also for therapeutic benefit.[128] Indeed, drug cocktails makeup a considerable portion of clinical treatments and are especially valuable in cancer therapy where drug combinations are often more efficacious than medicines used individually.[129] In this study, (-)-CXL017 demonstrates a synergy with three known SERCA inhibitors in the SERCA ATPase assay. While all combinations involving (-)-CXL017 are markedly synergistic, combinations of the known inhibitors are merely additive (Figure 3.5). This result was surprising given that TG, CPA, and BHQ bind at different sites within SERCA and exhibit different modes of inhibition. TG, CPA, and BHQ are known to lock SERCA in its E2 conformation upon binding in the TM domain, which lends to the notion that a small molecule that synergizes with one of these inhibitors likely synergizes with all of them.[95] Since (-)-CXL017 seems to interfere at or near the nucleotide binding domain in the cytoplasmic region, it is plausible that the conformational changes induced by (-)-CXL017 in the cytoplasmic headpiece are complementary to those induced by the TM inhibitors, thus potentiating the overall effect. Beyond the biochemical assay, synergy is also observed in cell viability experiments, specifically between (-)-CXL017 and TG, thus confirming the contribution of SERCA inhibition to the cytotoxicity of (-)-CXL017 in multidrug-resistant HL60/MX2 cells.

3.3. Conclusion

Small molecules targeting drug resistant cancers are of great clinical utility. In particular, molecules that maintain efficacy across cancers with unique mechanisms of resistance would be ideal. CXL017 was recently identified as a novel lead for the treatment of multidrug-resistant leukemia that demonstrates efficacy in several chemoresistant leukemia cell lines, despite varied modes of resistance. From the work presented in this chapter, CXL017 is shown to inhibit the ER Ca^{2+}-ATPase. Notable results include a synergistic profile that is upheld in cell viability assays, and a good correlation between SERCA inhibition and cell viability that is evident in the resistant (HL60/MX2) but not the parental (HL60) cell line. These findings suggest that SERCA is responsible for the susceptibility of HL60/MX2 to these inhibitors, and that inhibition of SERCA by CXLs may provide a novel route to target multidrug-resistant AML.

3.4. Materials and Methods

3.4.1. Reagents

All CXL molecules were synthesized as previously described. Thapsigargin was purchased from MP Biomedicals (Solon, OH). Cyclopiazonic acid, 2,5-di-*tert*-butylhydroquinone, and all other reagents including those used in the coupled enzyme assay for measuring ATP hydrolysis rates were of the highest purity available and purchased from Sigma-Aldrich (St. Louis, MO).

3.4.2. SERCA ATPase measurements and data analysis

Ca^{2+}-dependent ATPase activity was measured using light sarcoplasmic reticulum (LSR) vesicles purified from fast-twitch skeletal muscle of New Zealand white rabbits in a NADH-linked enzyme-coupled microtiter plate assay (200 uL/well) with free calcium ($[Ca^{2+}]$) tightly controlled using an EGTA buffering system as previously described.[130] Briefly, reaction buffer for the assay consisted of 5 mM $MgCl_2$, 100 mM KCl, 1 mM EGTA, 0.4 mM NADH, 10 IU/mL lactate dehydrogenase, 10 IU/mL pyruvate kinase, 7 ug/mL A23187 ionophore, and 50 mM MOPS at pH 7.0. The concentrations of lactate dehydrogenase and pyruvate kinase were varied to ensure that effects of compounds were not due to their effects on these enzymes. LSR protein was resuspended at 0.5 mg/mL. All reactions were conducted at 37 °C in duplicate or triplicate and results are reported as the mean of three independent experiments. ATP hydrolysis was determined as the rate of NADH oxidation, measured from the decay in absorbance at 340 nm using a Molecular Devices SpectraMax Plus spectrophotometer (Sunnyvale, CA). Compounds were introduced into the assay at their respective concentrations with 1% DMSO in the

final assay volume. All data fitting was carried out using GraphPad Prism software (San Diego, CA). In experiments where calcium was varied, ATPase activity was measured from pCa 5.0-7.5 while pATP was held contsant. The data were plotted (V vs pCa) and fitted by the Hill equation (Equation 3.1).

$$\boldsymbol{V = \frac{V_{max}}{1 + 10^{-n(pK_{Ca} - pCa)}}}$$

Equation 3.1. Hill equation

where V is the initial ATPase rate and n is the Hill coefficient. Data were normalized to the maximal rate, V_{max}, determined from the fit in the presence of 1% DMSO, and then replotted to assess changes in V_{max} and pK_{Ca} due to the added compound. In experiments where ATP was varied, ATPase activity was measured from pATP 2.6-6.4 while pCa was held constant. In this case, the data were plotted (V vs. pATP) and fitted by a Bi-Michaelis-Menten equation (Equation 3.2).

$$\boldsymbol{V = \frac{V_{max_{(cat)}}}{1 + 10^{(-pK_{ATP_{(cat)}} + pATP)}} + \frac{V_{max_{(reg)}}}{1 + 10^{(-pK_{ATP_{(reg)}} + pATP)}}}$$

Equation 3.2. Bi-Michaelis-Menten equation

where $V_{max(cat)}$ and p$K_{ATP(cat)}$ describe the catalytic ATP binding site and $V_{max(reg)}$ and p$K_{ATP(reg)}$ describe the regulatory ATP binding site. Data were normalized to the maximal rate, $V_{max(cat)}$, determined in the presence of 1% DMSO, and then plotted to assess changes in $V_{max(cat)}$, $V_{max(reg)}$, p$K_{ATP(cat)}$, and p$K_{ATP(reg)}$. As no significant change in

$V_{max(cat)}$ or $V_{max(reg)}$ was detected, these values were fixed to the values determined from control experiments and changes in p$K_{ATP(cat)}$ and p$K_{ATP(reg)}$ were ultimately determined. Lastly, in dose-response experiments where serial dilutions of each inhibitor were tested, pCa and pATP were held constant. Data were normalized to the enzyme rate determined in the presence of 1% DMSO, plotted (relative V vs. log[I]) and fitted with GraphPad Prism (San Diego, CA) according to a four-parameter dose-response equation with the Y_{min} and Y_{max} fixed to 0.5 and 1 respectively to accommodate comparison of the partial inhibitors. From the fit, the IC_{50} of each inhibitor was determined.

3.4.3. Evaluation of synergy in SERCA ATPase assay

Compounds (Figures 1.8 and 3.1) were introduced individually and in combination at a constant molar ratio to the ATPase assay. Data were processed using CompuSyn Software (Paramus, NJ) to determine the combination index (CI) based on the fraction of enzyme affected (f_a) by the individual inhibitors and their combinations. From the CI value, each inhibitor pair was characterized as synergistic (CI<0.9), additive (CI=0.9-1,1), or antagonistic (CI>1.1).[131] In the actual experiment, inhibitor ratios were determined experimentally to give f_a values ranging from 0.1-0.9 for individual inhibitors. Inhibitor concentrations were as follows: (-)-CXL017, 6.25 μM, 12.5 μM, and 25 μM; TG, 18.75 nM, 37.5 nM, and 75 nM; CPA, 0.16 μM, 0.31 μM, and 0.63 μM; BHQ, 0.31 μM, 0.63 μM, and 1.25 μM. Molar ratios were as follows: (-)-CXL017:TG, 667:1; (-)-CXL017:CPA, 80:1; (-)-CXL017:BHQ, 40:1; TG:CPA, 1:8.33; TG:BHQ, 1:16.7; CPA:BHQ, 1:2.

3.4.4. Cell cultures

HL60 cells were purchased from ATCC and grown in IMDM Glutamax medium (GIBCO, Carlsbad, CA) supplemented with 20% FBS. HL60/MX2 cells were also purchased from ATCC but grown in RPMI 1640 media (ATCC) supplemented with 10% FBS. Both cell lines were incubated at 37 °C under 5% CO_2 in air.

3.4.5. Cell viability measurement

Cytotoxicity was assessed by way of the CellTiter-Blue cell viability assay kit (Promega, Madison, WI) (see Section 2.4.9).[105] Similarly data were plotted and fit (Equation 2.1) to obtain the IC_{50} of each inhibitor.

3.4.6. Evaluation of synergy in cell culture

HL60/MX2 cells were plated in 24-well plates at $7.5x10^5$ cells/well and treated with (-)-CXL017, TG, or a combination thereof at a molar ratio of 667:1 in the presence of 1% DMSO. Following 16-hour incubation, 500 uL of each cell suspension was collected and centrifuged at 400xg for 4 minutes. After removing the media, cell pellets were resuspend in fresh media, transferred to individual wells of a 24-well plate, and allowed to incubate for additional 48 hours. Relative cell viability was assessed by trypan blue dye exclusion assay. Data were plotted as relative cell viability affected by each inhibitor or inhibitor combination.

CHAPTER 4

Investigation of CXL Bifunctional Photoaffinity Probes

4.1. Introduction

One of the major problems medicinal chemists encounter in the design of novel therapies is the identification of the intracellular targets of bioactive small molecules.[132] Even once the target is known, however, further investigation is often needed to elucidate the exact binding site within a given protein target in order to make informed decisions regarding the design of small molecules with improved affinity and specificity for the protein in question. One of the strategies for target and/or binding site characterization is the implementation of a photoaffinity (when not predisposed to covalent reactivity) probe based on chemical structure of the original bioactive hit, especially when the target protein is not amenable to x-ray crystallography or other specialized methods of structure determination.[133-135] Accordingly, photoaffinity labeling relies on introduction of a light-sensitive functionality into a parent molecule which facilitates formation of a covalent adduct between probe and protein, thus enabling down-stream target elucidation (Figure 4.1). Of these photo-reactive functionalities, aryl azides, benzophenones, and trifluoromethyldiazirines are most widely utilized.[136] Upon activation by UV light, each of these moieties undergoes transformation to a highly reactive intermediate that can participate in unique chemistries within the binding pocket of the host protein. In the case of aryl azides, loss of nitrogen leads to formation of a nitrene which is capable of a variety of reactions within the peptide backbone depending on the neighboring amino acid residues. With the probe covalently bound, additional chemistries and biochemical

techniques are employed to identify the probe-labeled protein, typically involving in-gel or in-membrane visualization following sodium dodecyl sulfate polyacrylamide gel electrophoresis (SDS-PAGE) as well as identification of tryptic peptides from the labeled protein (following gel-band excision and trypsin digestion) via tandem mass spectrometry (Figure 4.1).[137,138]

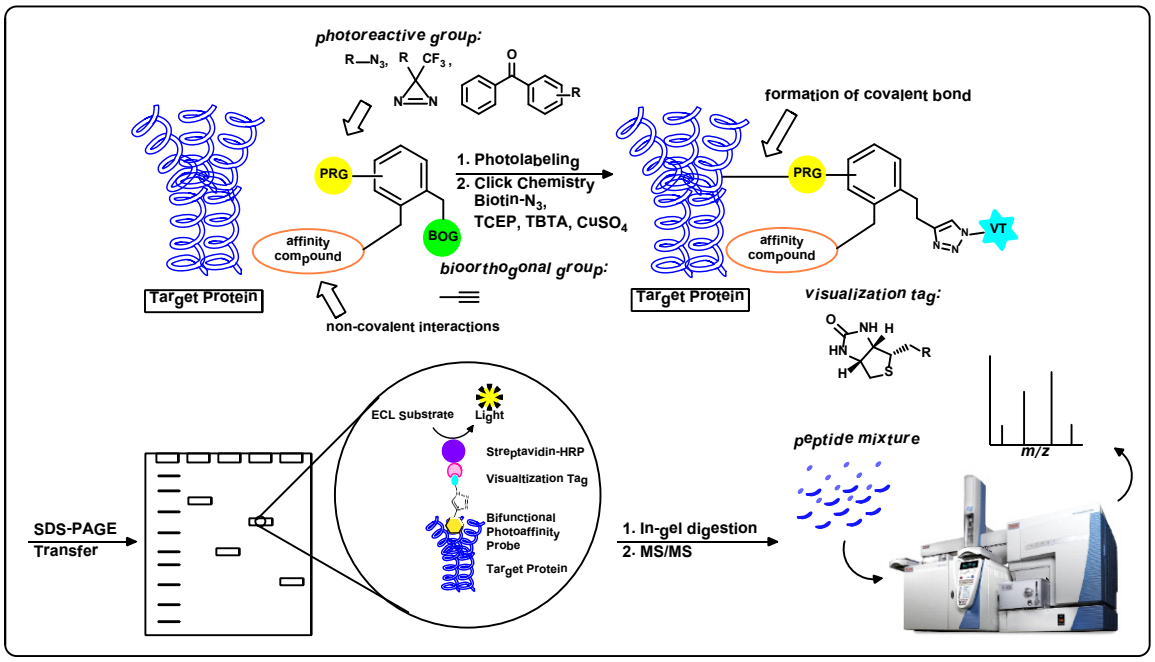

Figure 4.1. General outline of a photoaffinity-based pulldown experiment to investigate the binding site of a bioactive compound within a suspected target protein. TCEP: tris-(2-carboxyethyl)phosphine; TBTA: tris-(benzyltriazolylmethyl)amine.

In light of data supporting the inhibition of SERCA by CXLs, a photoaffinity based strategy was employed to determine the CXL binding site within the Ca^{2+}-ATPase. A series of photoaffinity probes were synthesized by incorporating both a light-sensitive functionality as well as a chemical handle for bioorthogonal conjugation to a suitable visualization agent via a copper-catalyzed 1,3-Husigen dipolar cycloaddition, better known as a 'Click' reaction. Performed at room temperature in aqueous solvent, the canonical 'Click' reaction involves the reaction of a monosubstituted alkyne with an organic azide to yield the corresponding 1,2,3 triazole, specifically the 1,4-disubstituted regioisomer.[139,140] With such inert reaction conditions, this transformation is amenable to most biological systems and is often the preferred route for introduction of a visualization or affinity tag to the chemical probe, since it can be carried out following adduction to the target protein (Figure 4.1).[141,142]

Though several probes were synthesized, incorporation of an aryl azide at the 6-position of the 4*H*-chromene scaffold proved ideal, whereas conversion of the 3 and/or 4 positions to propargyl esters for conjugation to an azido-biotin derivative via a 'Click' reaction was deemed appropriate based on the discovery of CXL070 (see Chapter 2). It was hypothesized that successful application of a CXL photoaffinity probe could be used to identify the exact binding location of CXLs within the calcium pump, thereby revealing the structural requirements for tighter binding as well as providing a molecular rationale for synergy observed with other SERCA inhibitors (see Chapter 3).

Preliminary labeling experiments with highly-purified SERCA enzyme, revealed CXL039 as the most suitable probe for labeling studies compared to (+)-CXL037 and (-)-

CXL037, based on in-membrane chemiluminescent band intensity generated upon biotin-recognition by streptavidin-horse radish peroxidase (HRP), analogous to a Western blot. Similar experimentation demonstrated that CXL039 was highly-specific for SERCA and did not readily label other purified and recombinant proteins. Furthermore, a clear dose-responsive labeling pattern was established with respect to the concentration of CXL039 and biotin azide. In agreement with data obtained in the SERCA activity assay, a reduction in band intensity was observed when competing agents – ATP and (-)-CXL017 - were introduced into the reaction mixture. Finally, cytotoxicity of (+)-CXL037, (-)-CXL037, and CXL039 was evaluated in both parental and MDR cell lines to determine the optimal system for future cell-based pull down experiments to further explore the molecular repertoire of CXL targets.

4.2. Results and Discussion

4.2.1. Design and synthesis of CXL photoaffinity probes (Performed by Dr. Balasubramanian Srinivasan and Dr. Aridoss Gopalakrishnan)

To generate bifunctional photoaffinity probes with limited structural modification relative to the parent compound, CXL017, only one transformation was added to the previously described synthetic route (see Chapter 2). Specifically, the 3' or 4' amino functionality present in CXL055 and CXL070 was reacted with trimethylsilylazide in the presence of *tert*-butylnitrite to afford the corresponding azidochromene derivatives.[143] CXL039 was prepared directly, whereas separation of the enantiomers of CXL055 by chiral HPLC yielded (+)-CXL055 and (-)-CXL055, which were subsequently transformed into the azido derivatives, (+)-CXL037 and (-)-CXL037 (Scheme 4.1).

Scheme 4.1. Synthetic route for the preparation of CXL photoaffinity probes

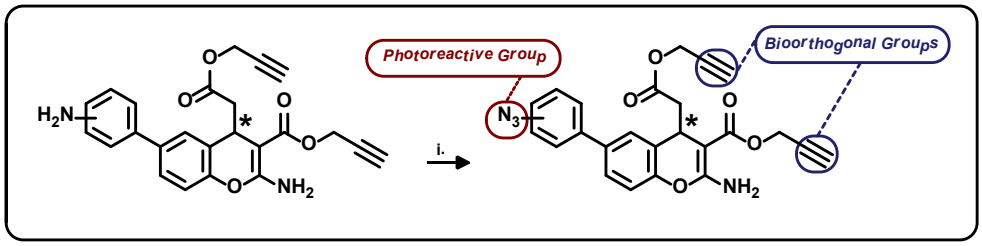

Reagents and conditions: (i) $TMSN_3$, *t*-BuONO, CH_3CN, 0 ^oC to rt, 4 h.

4.2.2. Photolabeling the sarco/endoplasmic reticulum Ca^{2+}-ATPase

Each of the three synthesized probes was evaluated for its ability to label SERCA. Labeling assays were carried out in four parts. First, probe molecules were allowed a short period of time to incubate with the ATPase (~3 ug) in reaction buffer to facilitate the initial binding between probe and protein. Second, the reaction mixture was illuminated by UV light (365 nm), providing the energy necessary for activation of the photophore. Each component for the 'Click' reaction was then added in the following sequence: biotin azide, tris(2-carboxyethyl)phosphine (TCEP), tris[(1-benzyl-1*H*-1,2,3-triazol-4-yl)methyl]amine (TBTA), and copper (II) sulfate. Accordingly, TCEP was responsible for reducing copper(II) to copper(I) and TBTA served as the copper ligand. In a final step, the protein was subjected to gel electrophoresis under reducing conditions and transferred to a polyvinylidene fluoride (PVDF) membrane for detection and visualization by streptavidin-HRP.

Initial experiments with (+)-CXL037, (-)-CXL037, and CXL039 indicated that the labeling observed was probe-, light-, and biotin-dependent (Figure 4.2 and 4.3B). A

faint band (lanes 3 and 4) was observed in the absence of light, though it was considerably weaker than the identical samples exposed to 365 nm UV (Lanes 7 and 8). Furthermore, CXL039 provided a stronger chemiluminescent signal compared to the enantiopure photoprobes, and was thus selected for further experimentation. Though (+)-CXL037 and (-)-CXL037 were particularly interesting in light of the enantiomeric preference observed with regards to cytotoxicity and SERCA inhibition (see Section 3.2.2), their indiscriminate labeling pattern negated their continued use for labeling of the ATPase.[108] Additional experiments with CXL039 demonstrated that the labeling of SERCA was concentration dependent (Figure 4.3A). A strong band at ~100 kDa was observed in the presence of 1 μM CXL039 that could be detected down to approximately 60 nM. The concentration of biotin was also critical. After some optimization, 25 μM biotin azide was selected for continued studies based on the observed dose-response (Figure 4.3B). To relate inhibition in the enzymatic assay, an important experiment was carried out, again with CXL039, wherein (-)-CXL017 and ATP were introduced into the labeling mixture. Both of these competitors exhibited attenuated the extent of labeling by CXL039, providing evidence that the binding site of the probe was indeed the same as that of the (-)-CXL017 (Figure 4.4).

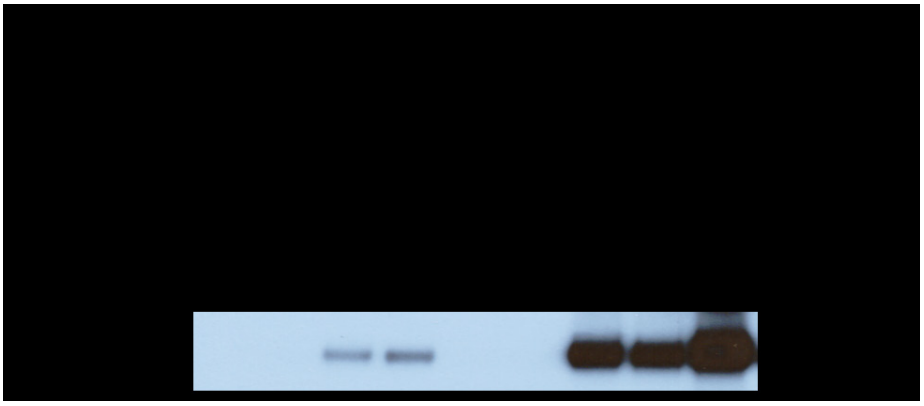

Figure 4.2. Photolabeling of purified SERCA protein with CXL photoprobes. (+)-CXL037, (-)-CXL037, and CXL039 were introduced into the labeling reaction mixture with SERCA protein at a concentration of 10 μM. Following 30 min incubation and exposure to 365 nm light (indicated samples only), biotin was conjugated to the probe-protein complex via a 'Click' reaction. The protein was subjected to SDS-PAGE, transferred to PVDF membrane, and visualized with a streptavidin-HRP conjugate. The chemiluminescent signal was detected by x-ray film. Figure is representative of two independent experiments.

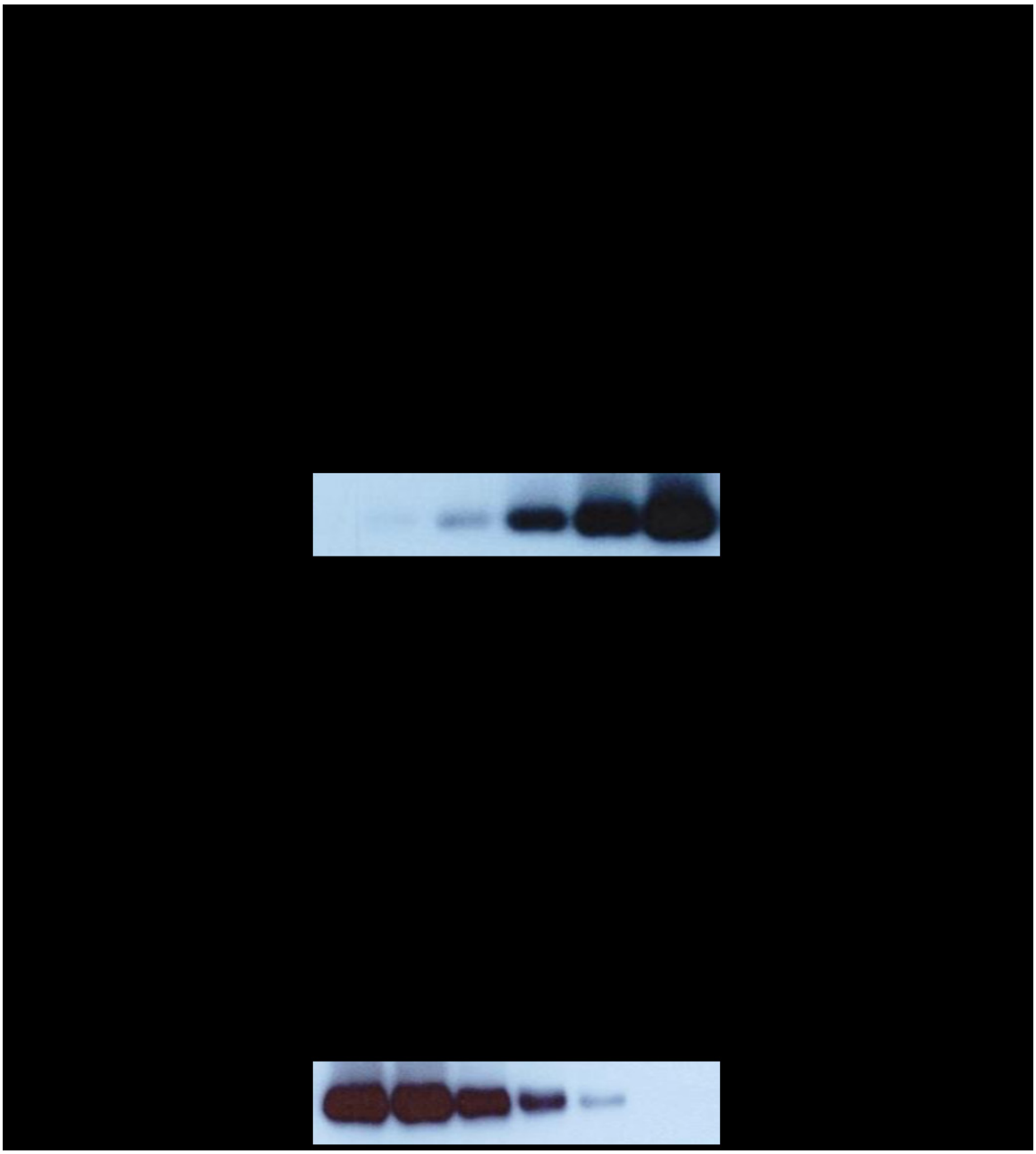

Figure 4.3. Photolabeling of purified SERCA protein with CXL039. CXL039 and Biotin-N_3 were introduced into the SERCA labeling reaction at the indicated concentrations. (A) The concentration of CXL039 was varied from 0.03125 μM to 1 μM in the presence of 25 μM Biotin-N_3. (B) The concentration of Biotin-N_3 was varied from 6.25 μM to 100 μM in the presence of 1 μM CXL039. Following 30 min incubation and

exposure to 365 nm light (indicated samples only), biotin was conjugated to the probe-protein complex via a 'Click' reaction. The protein was subjected to SDS-PAGE, transferred to PVDF membrane, and visualized with a streptavidin-HRP conjugate. The chemiluminescent signal was detected by x-ray film. Figure is representative of two independent experiments.

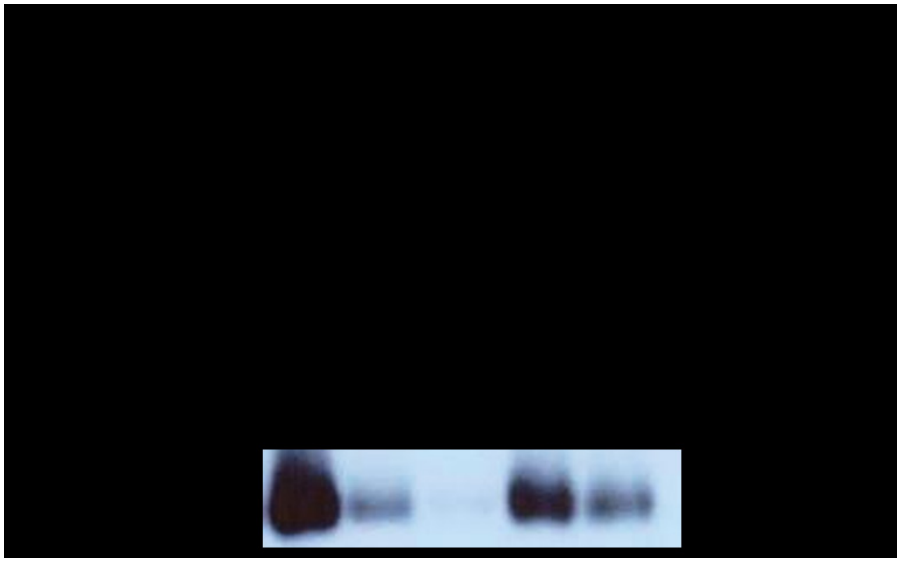

Figure 4.4. Photolabeling of purified SERCA protein by CXL039 in the presence of CXL017 and ATP. CXL039 (1 μM) and Biotin-N_3 (25 μM) were introduced into the SERCA labeling reaction in the presence of either ATP or (-)-CXL017 at the indicated concentrations. Following 30 min incubation and exposure to 365 nm light, biotin was conjugated to the probe-protein complex via a 'Click' reaction. The protein was subjected to SDS-PAGE, transferred to PVDF membrane, and visualized with a streptavidin-HRP conjugate. The chemiluminescent signal was detected by x-ray film. Figure is representative of three independent experiments.

An important consideration of any affinity labeling experiment is the specificity of protein labeling. With encouraging data related to SERCA labeling by CXL039, the specificity of this probe was evaluated by introducing a variety of recombinant and purified proteins into the labeling reaction. Proteins of varying molecular weight (20-60 kDa) and physiochemical properties were selected. A total of eight proteins were investigated for non-specific labeling including Bcl-2, Mcl-1, bovine serum albumin (BSA), dimeric dihydrofolate reductase (1DD), human histidine triad nucleotide-binding protein 2 (hHint2), mycobacterium tuberculosis salicylate synthase (MbtI), TEM1 β-lactmase, and vancomycin resistance D-Ala-D-Ala dipeptidase (VanX). In the presence of these proteins, CXL039 demonstrated highly specific labeling of SERCA (Figure 4.5). While the protein band at ~100 kDa was unaffected, the emergence of any new bands corresponding to one of the other proteins was not detected. It is interesting that CXL039 did not label either Bcl-2 or Mcl-1 considering previous data that implicated a role for these proteins in the mechanism of CXL-induced cell death.[107] In addition, previous evidence indicated a physical interaction between Bcl-2 and SERCA.[49] However, since the Bcl-2 and Mcl-1 proteins used in this experiment were truncated forms, they may have lacked the structural components necessary for SERCA interaction and/or antagonism by CXLs. It is also plausible that CXLs do not inhibit Bcl-2 or Mcl-1 directly, but that signal transduction or feedback processes contribute to the ability of CXLs to alter the expression of Bcl-2 family proteins *in vitro*.

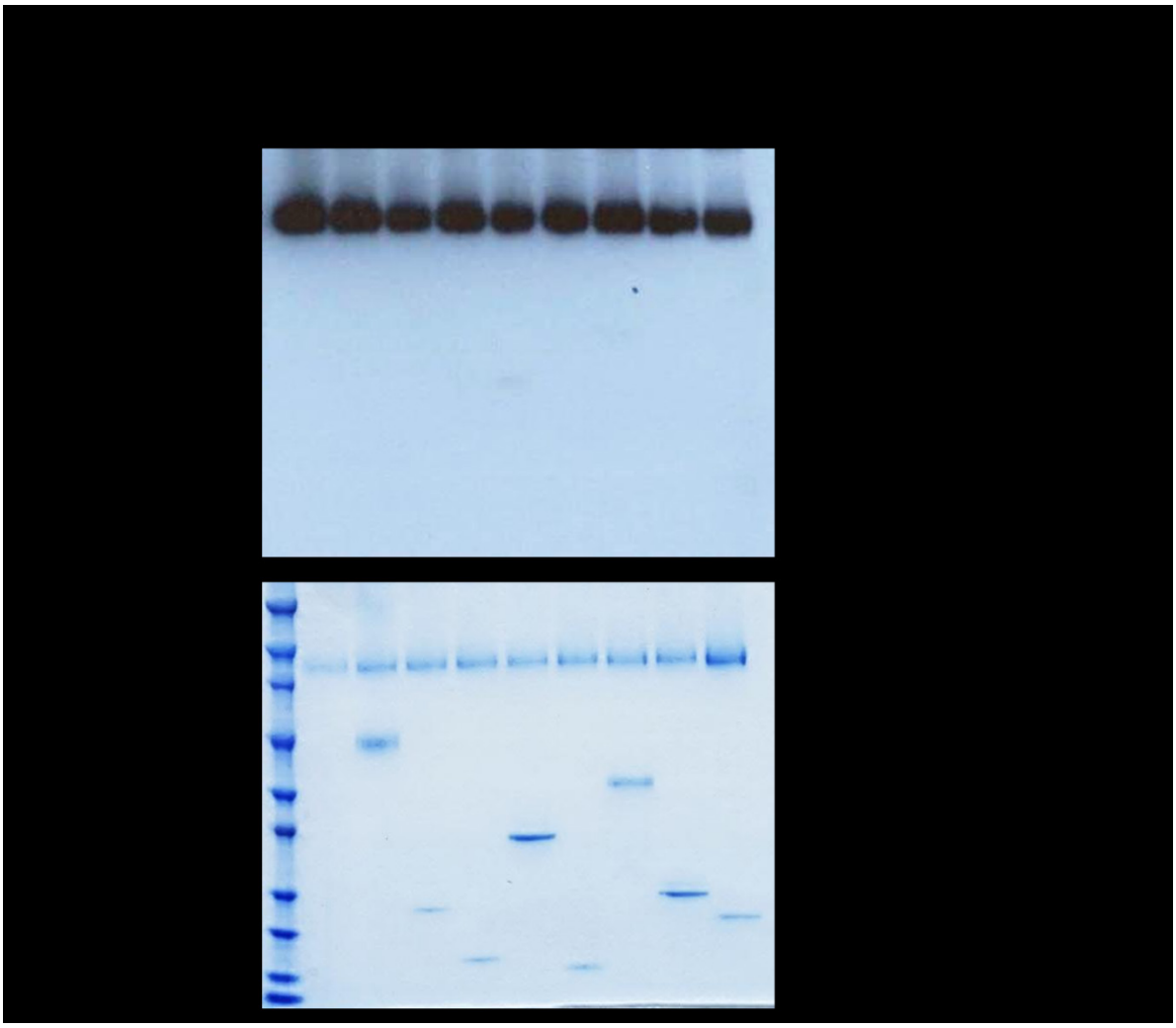

Figure 4.5. Photolabeling of purified SERCA protein by CXL039 in the presence of recombinant or purified protein. CXL039 (1 μM) and Biotin-N_3 (25 μM) were introduced into the labeling reaction containing SERCA alone or in the presence of another recombinant or purified protein (indicated in figure). The concentration of each protein was 1 μM. Following 30 min incubation and exposure to 365 nm light, biotin was conjugated to the probe-protein complex via a 'Click' reaction. (A) The protein was subjected to SDS-PAGE, transferred to PVDF membrane, and visualized with a streptavidin-HRP conjugate. The chemiluminescent signal was detected by x-ray film.

(B) Following SDS-PAGE, total protein was stained by Coomassie blue to provide colorimetric detection. Figure is representative of two independent experiments.

4.2.3. Cytotoxicity of photoaffinity probes in parental and MDR cancer cells

Having demonstrated the utility of CXL-based photoaffinity probes for labeling SERCA, it was reasoned that a similar strategy could be used to identify intracellular targets beyond the ER calcium pump. Prior to implementing a cell-based pull-down experiment, a cytotoxicity screen was completed to determine the efficacy of photoaffinity probes in four sets of parental and MDR cancer cell lines. Specifically, (+)-CXL037, (-)-CXL037, and CXL039 were evaluated in HL60/MX2, HL60/ADR, HL60/DNR, HL60/DOX, and K562/DOX as well as the corresponding parental cell lines (for descriptions of these cell lines see Section 2.4.8) (Figure 4.6). Each of the photoaffinity probes behaved similarly to their non-light sensitive counterparts with regard to the overall trend. (+)-CXL037 was inactive across the entire cell line panel. (-)-CXL037, on the other hand possessed good activity with a low-micromolar recorded IC_{50} in all 5 MDR cell lines. CXL039 performed better than (+)-CXL037 but not as well as (-)-CXL037. Analysis of the bioactive probes in the parental cell lines versus the MDR lines revealed approximately equipotent activity, in agreement with the activity profile of the most recent lead in the CXL series, CXL070.[126] Future target deconvolution via cell-based pull down experiments will benefit from the sharp contrast in potency between (+)-CXL037 and (-)-CXL037. Ideally, (-)-CXL037 will reveal specific, high-priority protein targets, while (+)-CXL037 will aid in the determination of

non-specific binding partners, providing a streamlined route to the identification of novel molecular targets of CXLs.

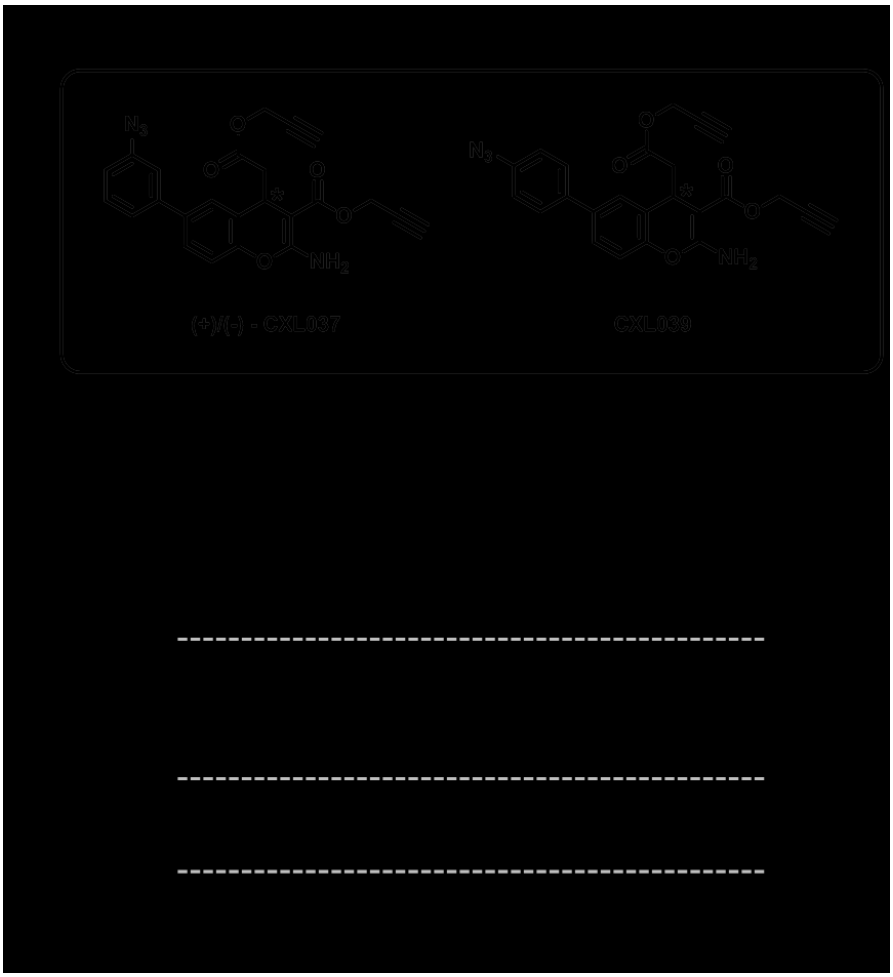

Figure 4.6. Cytotoxicity of CXL photoaffinity probes in MDR and parental cancer cells. (+)-CXL037, (-)-CXL037, and CXL039 were evaluated in a cell viability assay in the indicated cell lines. The IC_{50} of each probe was determined by a fit of the respective dose-response curves to the four-parameter dose-response equation (Equation 2.1). (A) Chemical structures of CXL photoaffinity probes. (B) IC_{50} values of photoprobes in parental and corresponding MDR cell lines. Since these cell lines originiate from different sources (see Section 2.4), the parental cell lines with the same designation do

not demonstrate equialent sensitivity to the same small molecule. Data are expressed as mean ± SEM, n = 3. Figure is representative of three independent experiments.

4.3. Conclusion

In this final chapter, a set of photoaffinity molecules based on the CXL scaffold were synthesized and purposed to elucidate the CXL binding site within SERCA. Preliminary labeling experiments with (+)-CXL037, (-)-CXL037, and CXL039 indicated that CXL039 provided the strongest labeling signal and that labeling was dependent on light and biotin – introduced by a 'Click' reaction. Additionally, CXL039 labeled SERCA in a dose-responsive manner and was shown to compete with (-)-CXL017 and ATP for binding to the ATPase. Aside from the labeling of purified protein, the cytotoxicity of (+)-CXL037, (-)-CXL037, and CXL039 was evaluated in parental and MDR cells. (-)-CXL037 proved to the most efficacious cytotoxin among the photoprobes followed by CXL039 and (+)-CXL037, the latter of which did not induce cell killing at concentrations up to 50 μM. These data support continued investigation of CXL-based probes to uncover the preferred binding pocket within the ER Ca^{2+}-ATPase as well as other potential cellular targets of CXLs, ultimately leading to more effective medicinal agents targeting MDR cancer.

4.4. Materials and Methods

4.4.1. Chemistry

CXL photoaffinity probes were synthesized by Dr. Balasubramanian Srinivasan and Dr. Aridoss Gopalakrishnan based on an established protocol with CXL055 and CXL070 as precursors.[143] HPLC separation of the enantiomers of CXL055 was performed by Regis Technologies (Morton Grove, IL). All commercial reagents and anhydrous solvents were purchased from vendors and were used without further purification or distillation unless otherwise stated. Analytical thin layer chromatograph was performed on Whatman silica gel 60 Å with fluorescent indicator (partisil K6F). Flash column chromatography was performed on Whatman silica gel 60 Å (230−400 mesh). NMR (^{1}H and ^{13}C) spectra were recorded on a Varian or Bruker 400 MHz spectrometer and calibrated using an internal reference. ESI mode mass spectra were recorded on a Agilent MSD SL ion trap or Bruker BiotofII mass spectrometer.

4.4.2. General procedure for the conversion of aromatic amines into azides[143]

The 3' or 4'-aryl chromene (1 eq.) was dissolved in CH_3CN (3-5 mL) in a 25 mL round-bottomed flask and cooled to 0°C in an ice bath. To this stirred mixture was added *t*-BuONO (1.5 eq.) followed by $TMSN_3$ (1.2 eq.) dropwise. The resulting solution was stirred at room temperature for 4 h. The reaction mixture was concentrated under vacuum and the crude mass was purified by column chromatography to give the product.

4.4.3. Reagents

Biotin Azide (PEG4 carboxamide-6-azidohexanyl biotin) and SimplyBlue SafeStain (Coomassie-G250) were purchased from Life Technologies (Carlsbad, CA).

Ultrasensitive streptavidin−peroxidase polymer was purchased from Sigma-Aldrich (St. Louis, MO). Lastly, SuperSignal West Pico Chemiluminescent Substrate was supplied by Thermo Fisher (Rockford, IL). Proteins for evaluation of probe specificity were provided or purchased from the following sources: BSA (Sigma-Aldrich), truncated Bcl-2 (Dr. Jialing Lin, University of Oklahoma), truncated Mcl-1 (Dr. Sonia Das, University of Minnesota), 1DD (Amit Gangar, University of Minnesota), hHint2 (Rachit Shah, University of Minnesota), MbtI, TEM1, and VanX (Kimberly Maize, University of Minnesota). All other reagents including tris-(2-carboxyethyl)phosphine (TCEP) and tris-(benzyltriazolylmethyl)amine (TBTA) for the 'Click' reaction were of the highest purity available and purchased from Sigma-Aldrich (St. Louis, MO). The reagents and equipment for SDS-PAGE included NuPAGE Novex 4-12% Bis-Tris precast polyacrylamide gels, NuPAGE MOPS Running Buffer, and NuPAGE Transfer Buffer and were purchased from Life Technologies (Carlsbad, CA).

4.4.4. Purification of SERCA protein (performed by members of the Thomas lab)

SERCA was purified from skeletal muscle of New Zealand white rabbits in 0.01% $C_{12}E_8$ by the Reactive-Red method and then flash-frozen and stored in liquid nitrogen after addition of 0.5 mg of lipid (sonicated DOPC and DOPE, 4:1 ratio by weight) /mg of protein.[125,144] Protein concentration was determined by the bicinchoninic acid assay (BCA), using bovine serum albumin as the standard.

4.4.5. General protocol for photolabeling of purified SERCA protein

Photolabeling experiments were performed in individual wells of a 96-well pointed-bottom plate. First, protein was taken in reaction buffer (5 mM $MgCl_2$, 100 mM KCl, 1 mM EGTA, and 50 mM MOPS at pH 7.0) at a concentration of 1 μM (M.W. 100 kDa) and allowed to incubate at room temperature for 30 min with probe molecules in the presence of 10% DMSO. In cases when competing small molecules or additional proteins were present, extra components were added as well, with the total reaction volume held constant. Next, the plate was cooled to 0 °C and samples were subjected to 365 nm light from a handheld lamp for 10 min. The lamp was placed directly atop the 96-well plate with samples centered in the path of light. Following UV irradiation, 'Click' reagents were added in the following order to yield the final indicated concentrations: Biotin-N_3 (25 μM, unless otherwise noted), TCEP (1 mM), TBTA (200 μM), $CuSO_4$ (1 mM). Samples were subsequently incubated in the plate for an additional 1 h. After the incubation period, samples for SDS-PAGE (reducing conditions) were prepared from aliquots of the individual reaction mixtures. Gel electrophoresis was performed at 150 V for 1.5 h. In certain experiments, total protein was stained in-gel with Coomassie G-250 following the manufacturer's protocol. In most cases, however, transfer of protein from the gel to PVDF membrane was performed at 40 V for 3 h. The membrane was blocked with 1% BSA in PBST (PBS with 0.05% TWEEN20) and incubated with ultra-sensitive streptavidin-peroxidase polymer for 1 h at room temperature. Prior to use, the streptavidin conjugate was diluted 1:10000 in PBST.

Finally, biotinylated protein was visualized upon addition of a chemiluminescent peroxidase substrate. Resultant luminescence was captured using x-ray film.

4.4.6. Cell cultures

All cell lines were grown in RPMI 1640 media (ATCC) supplemented with 10% FBS and incubated at 37 °C under 5% CO_2 in air. Detailed information regarding the original source and development of HL60/MX2, HL60/ADR, HL60/DNR, HL60/DOX, and K562/DOX as well as the corresponding parental cell lines was described previously (see Section 2.4.8).

4.4.7. Cell viability measurement

Cytotoxicity was assessed by way of the CellTiter-Blue cell viability assay kit (Promega, Madison, WI) (see Section 2.4.9).[105] Similarly data were plotted and fit (Equation 2.1) to obtain the IC_{50} of each inhibitor.

1 Hanahan, D. & Weinberg, R. A. Hallmarks of cancer: the next generation. *Cell* **144**, 646-674 (2011).
2 Stratton, M. R., Campbell, P. J. & Futreal, P. A. The cancer genome. *Nature* **458**, 719-724 (2009).
3 Vogelstein, B. *et al.* Cancer genome landscapes. *Science* **339**, 1546-1558 (2013).
4 Hanash, S. & Taguchi, A. The grand challenge to decipher the cancer proteome. *Nat. Rev. Cancer* **10**, 652-660 (2010).
5 Jones, D. S., Podolsky, S. H. & Greene, J. A. The burden of disease and the changing task of medicine. *New Engl. J. Med.* **366**, 2333-2338 (2012).
6 Siegel, R. *et al.* Cancer treatment and survivorship statistics, 2012. *CA-Cancer J. Clin.* **62**, 220-241 (2012).
7 Siegel, R., Naishadham, D. & Jemal, A. Cancer statistics, 2013. *CA-Cancer J. Clin.* **63**, 11-30 (2013).
8 Fojo, T. & Bates, S. Strategies for reversing drug resistance. *Oncogene* **22**, 7512-7523 (2003).
9 Gottesman, M. M. Mechanisms of cancer drug resistance. *Annu. Rev. Med.* **53**, 615-627 (2002).
10 Gillet, J.-P. & Gottesman, M. in *Multi-Drug Resistance in Cancer* Vol. 596 *Methods in Molecular Biology* (ed Jun Zhou) Ch. 4, 47-76 (Humana Press, 2010).
11 Shipley, J. L. & Butera, J. N. Acute myelogenous leukemia. *Exp. Hematol.* **37**, 649-658 (2009).
12 Farag, S. S. *et al.* Outcome of induction and postremission therapy in younger adults with acute myeloid leukemia with normal karyotype: a cancer and leukemia group B study. *J. Clin. Oncol.* **23**, 482-493 (2005).
13 Dillman, R. O. *et al.* A comparative study of two different doses of cytarabine for acute myeloid leukemia: a phase III trial of cancer and leukemia group B. *Blood* **78**, 2520-2526 (1991).
14 Pastan, I. & Gottesman, M. Multiple-drug resistance in human cancer. *N. Engl. J. Med.* **316**, 1388-1481 (1987).
15 Baguley, B. Multiple drug resistance mechanisms in cancer. *Mol. Biotechnol.* **46**, 308-316 (2010).
16 Szer, J. The prevalent predicament of relapsed acute myeloid leukemia. *ASH Education Program Book* **2012**, 43-48 (2012).
17 Sawyers, C. L. Cancer: mixing cocktails. *Nature* **449**, 993-996 (2007).
18 Persidis, A. Cancer multidrug resistance. *Nat Biotechnol.* **17**, 94-95 (1999).
19 Longley, D. B. & Johnston, P. G. Molecular mechanisms of drug resistance. *J. Pathol.* **205**, 275-292 (2005).
20 Gottesman, M. M., Fojo, T. & Bates, S. E. Multidrug resistance in cancer: role of ATP-dependent transporters. *Nat. Rev. Cancer* **2**, 48-58 (2002).
21 Membrane transporters in drug development. *Nat. Rev. Drug Discov.* **9**, 215-236 (2010).
22 Schinkel, A. H. & Jonker, J. W. Mammalian drug efflux transporters of the ATP binding cassette (ABC) family: an overview. *Adv. Drug Delivery Rev.* **64,** 138-153 (2012).

23 Loo, T. W. & Clarke, D. M. Recent progress in understanding the mechanism of P-glycoprotein-mediated drug efflux. *J. Membrane Biol.* **206**, 173-185 (2005).
24 Li, Y. *et al.* The structure and functions of P-glycoprotein. *Curr. Med. Chem.* **17**, 786-800 (2010).
25 Ferrao, P., Sincock, P., Cole, S. & Ashman, L. Intracellular P-gp contributes to functional drug efflux and resistance in acute myeloid leukaemia. *Leukemia Res.* **25**, 395-405 (2001).
26 Sharom, F. J. The P-glycoprotein efflux pump: how does it transport drugs? *J. Membrane Biol.* **160**, 161-175 (1997).
27 Mahadevan, D. & List, A. F. Targeting the multidrug resistance-1 transporter in AML: molecular regulation and therapeutic strategies. *Blood* **104**, 1940-1951 (2004).
28 Szakacs, G., Paterson, J. K., Ludwig, J. A., Booth-Genthe, C. & Gottesman, M. M. Targeting multidrug resistance in cancer. *Nat. Rev. Drug Discov.* **5**, 219-234 (2006).
29 Boesch, D. *et al.* In vivo circumvention of P-glycoprotein-mediated multidrug resistance of tumor cells with SDZ PSC 833. *Cancer Res.* **51**, 4226-4233 (1991).
30 Fox, E. & Bates, S. E. Tariquidar (XR9576): a P-glycoprotein drug efflux pump inhibitor. *Expert Rev. of Anticancer Ther.* **7**, 447-459 (2007).
31 Dantzig, A. H. *et al.* Reversal of P-glycoprotein-mediated multidrug resistance by a potent cyclopropyldibenzosuberane modulator, LY335979. *Cancer Res.* **56**, 4171-4179 (1996).
32 Binkhathlan, Z. & Lavasanifar, A. P-glycoprotein inhibition as a therapeutic approach for overcoming multidrug resistance in cancer: current status and future perspectives. *Curr. Cancer Drug Targets* **13**, 326-346 (2013).
33 Hall, M. D. *et al.* Synthesis, activity, and pharmacophore development for isatin-*β*-thiosemicarbazones with selective activity toward multidrug-resistant cells. *J. Med. Chem.* **52**, 3191-3204 (2009).
34 Hall, M. *et al.* Synthesis and structure-activity evaluation of isatin-*β*-thiosemicarbazones with improved selective activity toward multidrug-resistant cells expressing P-glycoprotein. *J. Med. Chem.* **54**, 5878-5889 (2011).
35 Kang, M. H. & Reynolds, C. P. Bcl-2 inhibitors: targeting mitochondrial apoptotic pathways in cancer therapy. *Clin. Cancer Res.* **15**, 1126-1132 (2009).
36 Cotter, T. G. Apoptosis and cancer: the genesis of a research field. *Nat. Rev. Cancer* **9**, 501-507 (2009).
37 Kluck, R. M., Bossy-Wetzel, E., Green, D. R. & Newmeyer, D. D. The release of cytochrome C from mitochondria: a primary site for Bcl-2 regulation of apoptosis. *Science* **275**, 1132-1136 (1997).
38 Häcki, J. *et al.* Apoptotic crosstalk between the endoplasmic reticulum and mitochondria controlled by Bcl-2. *Oncogene* **19**, 2286-2295 (2000).
39 Chipuk, J. E., Moldoveanu, T., Llambi, F., Parsons, M. J. & Green, D. R. The BCL-2 family reunion. *Mol. Cell* **37**, 299-310 (2010).
40 Gross, A., McDonnell, J. & Korsmeyer, S. BCL-2 family members and the mitochondria in apoptosis. *Gene Dev.* **13**, 1899-1911 (1999).

41 Letai, A. G. Diagnosing and exploiting cancer's addiction to blocks in apoptosis. *Nat. Rev. Cancer* **8**, 121-132 (2008).
42 Certo, M. *et al.* Mitochondria primed by death signals determine cellular addiction to antiapoptotic BCL-2 family members. *Cancer Cell* **9**, 351-365 (2006).
43 Letai, A. *et al.* Distinct BH3 domains either sensitize or activate mitochondrial apoptosis, serving as prototype cancer therapeutics. *Cancer Cell* **2**, 183-192 (2002).
44 Cheng, E. *et al.* BCL-2, BCL-X_L sequester BH3 domain-only molecules preventing BAX- and BAK-mediated mitochondrial apoptosis. *Mol. Cell* **8**, 705-711 (2001).
45 Fulda, S. & Debatin, K. M. Extrinsic versus intrinsic apoptosis pathways in anticancer chemotherapy. *Oncogene* **25**, 4798-4811 (2006).
46 Demaurex, N. & Distelhorst, C. Apoptosis-the calcium connection. *Science* **300**, 65-67 (2003).
47 Rong, Y. & Distelhorst, C. Bcl-2 protein family members: versatile regulators of calcium signaling in cell survival and apoptosis. *Annu. Rev. Physiol.* **70**, 73-164 (2008).
48 Eckenrode, E., Yang, J., Velmurugan, G., Foskett, J. & White, C. Apoptosis protection by Mcl-1 and Bcl-2 modulation of inositol 1,4,5-trisphosphate receptor-dependent Ca^{2+} signaling. *J. Biol. Chem.* **285**, 13678-13762 (2010).
49 Dremina, E. *et al.* Anti-apoptotic protein Bcl-2 interacts with and destabilizes the sarcoplasmic/endoplasmic reticulum Ca^{2+}-ATPase (SERCA). *Biochem. J.* **383**, 361-431 (2004).
50 Monteith, G., McAndrew, D., Faddy, H. & Roberts-Thomson, S. Calcium and cancer: targeting Ca^{2+} transport. *Nat. Rev. Cancer* **7**, 519-530 (2007).
51 Berridge, M., Bootman, M. & Roderick, H. Calcium signalling: dynamics, homeostasis and remodelling. *Nat. Rev. Mol. Cell Biol.* **4**, 517-529 (2003).
52 Rizzuto, R. *et al.* Calcium and apoptosis: facts and hypotheses. *Oncogene* **22**, 8619-8627 (2003).
53 Johnstone, R., Ruefli, A. & Lowe, S. Apoptosis: a link between cancer genetics and chemotherapy. *Cell* **108**, 153-164 (2002).
54 Reed, J. Bcl-2 family proteins: regulators of chemoresistance in cancer. *Toxicol. Lett.* **82-83**, 155-158 (1995).
55 Placzek, W. J. *et al.* A survey of the anti-apoptotic Bcl-2 subfamily expression in cancer types provides a platform to predict the efficacy of Bcl-2 antagonists in cancer therapy. *Cell Death Dis* **1**, e40 (2010).
56 Yip, K. W. & Reed, J. C. Bcl-2 family proteins and cancer. *Oncogene* **27**, 6398-6406 (2008).
57 Tzifi, F. *et al.* The role of BCL2 family of apoptosis regulator proteins in acute and chronic leukemias. *Adv. Hematol.* **2012**, 15 (2012).
58 Karakas, T. *et al.* High expression of bcl-2 mRNA as a determinant of poor prognosis acute myeloid leukemia. *Ann. Oncol.* **9**, 159-165 (1998).

59 Campos, L. *et al.* High expression of bcl-2 protein in acute myeloid leukemia cells is associated with poor response to chemotherapy. *Blood* **81**, 3091-3096 (1993).
60 Amundson, S. A. *et al.* An informatics approach identifying markers of chemosensitivity in human cancer cell lines. *Cancer Res.* **60**, 6101-6110 (2000).
61 Del Poeta, G. *et al.* Amount of spontaneous apoptosis detected by Bax/Bcl-2 ratio predicts outcome in acute myeloid leukemia (AML). *Blood* **101**, 2125-2131 (2003).
62 Minagawa, N. *et al.* The anti-apoptotic protein Mcl-1 inhibits mitochondrial Ca^{2+} signals. *J. Biol. Chem.* **280**, 33637-33644 (2005).
63 Glaser, S. P. *et al.* Anti-apoptotic Mcl-1 is essential for the development and sustained growth of acute myeloid leukemia. *Gene Dev.* **26**, 120-125 (2012).
64 Bose, P. & Grant, S. Mcl-1 as a therapeutic target in acute myelogenous leukemia (AML). *Leukemia Res. Reports* **2**, 12-14 (2013).
65 Lessene, G., Czabotar, P. E. & Colman, P. M. BCL-2 family antagonists for cancer therapy. *Nat. Rev. Drug Discov.* **7**, 989-1000 (2008).
66 Billard, C. Design of novel BH3 mimetics for the treatment of chronic lymphocytic leukemia. *Leukemia* **26**, 2032-2038 (2012).
67 Zhai, D., Jin, C., Satterthwait, A. & Reed, J. Comparison of chemical inhibitors of antiapoptotic Bcl-2-family proteins. *Cell Death Diff.* **13**, 1419-1421 (2006).
68 James, D. *et al.* AT-101, a small molecule Bcl-2 antagonist, in treatment naive CLL patients (pts) with high risk features; Preliminary results from an ongoing phase I trial. *J. Clin. Oncol.* **24**, 6605 (2006).
69 Petros, A. M. *et al.* Discovery of a potent and selective Bcl-2 inhibitor using SAR by NMR. *Bioorg. Med. Chem. Lett.* **20**, 6587-6591 (2010).
70 Xiao, G., Fang, H., Xing, C. & Xu, W. Structure, function, and inhibition of Bcl-2 family proteins: a new target for anti-tumor agents. *Mini Rev. Med. Chem.* **9**, 1596-1604 (2009).
71 Oltersdorf, T. *et al.* An inhibitor of Bcl-2 family proteins induces regression of solid tumours. *Nature* **435**, 677-681 (2005).
72 Schimmer, A. *et al.* A phase I study of the pan bcl-2 family inhibitor obatoclax mesylate in patients with advanced hematologic malignancies. *Clin. Cancer Res.* **14**, 8295-8301 (2008).
73 Souers, A. J. *et al.* ABT-199, a potent and selective BCL-2 inhibitor, achieves antitumor activity while sparing platelets. *Nat. Med.* **19**, 202-208 (2013).
74 Carafoli, E. The calcium-signalling saga: tap water and protein crystals. *Nat. Rev. Mol. Cell Biol.* **4**, 326-332 (2003).
75 Clapham, D. E. Calcium Signaling. *Cell* **131**, 1047-1058 (2007).
76 Hajnóczky, G. *et al.* Mitochondrial calcium signalling and cell death: approaches for assessing the role of mitochondrial Ca^{2+} uptake in apoptosis. *Cell Calcium* **40**, 553-560 (2006).
77 Pinton, P., Giorgi, C., Siviero, R., Zecchini, E. & Rizzuto, R. Calcium and apoptosis: ER-mitochondria Ca^{2+} transfer in the control of apoptosis. *Oncogene* **27**, 6407-6418 (2008).

78 Nakamura, K. *et al.* Changes in endoplasmic reticulum luminal environment affect cell sensitivity to apoptosis. *J. Cell Biol.* **150**, 731-740 (2000).
79 Pinton, P. *et al.* The Ca^{2+} concentration of the endoplasmic reticulum is a key determinant of ceramide-induced apoptosis: significance for the molecular mechanism of Bcl-2 action. *EMBO J.* **20**, 2690-2701 (2001).
80 Orrenius, S., Zhivotovsky, B. & Nicotera, P. Regulation of cell death: the calcium-apoptosis link. *Nat. Rev. Mol. Cell Biol.* **4**, 552-565 (2003).
81 Distelhorst, C. W. & Shore, G. C. Bcl-2 and calcium: controversy beneath the surface. *Oncogene* **23**, 2875-2880 (2004).
82 Dremina, E. S., Sharov, V. S. & Schöneich, C. Heat-shock proteins attenuate SERCA inactivation by the anti-apoptotic protein Bcl-2: possible implications for the ER Ca^{2+}-mediated apoptosis. *Biochem. J.* **444**, 127-139 (2012).
83 Janssen, K. *et al.* Inhibition of the ER Ca^{2+} pump forces multidrug-resistant cells deficient in Bak and Bax into necrosis. *J.Cell Sci.* **122**, 4481-4491 (2009).
84 Wong, V. K. *et al.* Saikosaponin-d, a novel SERCA inhibitor, induces autophagic cell death in apoptosis-defective cells. *Cell Death Dis.* **4**, e720 (2013).
85 Sulová, Z. *et al.* Does any relationship exist between P-glycoprotein-mediated multidrug resistance and intracellular calcium homeostasis. *Gen. Physiol. Biophys.* **28**, F89-F95 (2009).
86 Schlemmer, S., Yang, C. & Sirotnak, F. Functional modulation of multidrug resistance-related P-glycoprotein by Ca^{2+}-calmodulin. *J. Biol. Chem.* **270**, 11040-11042 (1995).
87 Kawakami, M. *et al.* Knock-down of sorcin induces up-regulation of MDR1 in HeLa cells. *Biol. Pharm. Bull.* **30**, 1065-1073 (2007).
88 Tan, Y. *et al.* Expression of sorcin predicts poor outcome in acute myeloid leukemia. *Leukemia Res.* **27**, 125-131 (2003).
89 Seres, M. *et al.* Overexpression of P-glycoprotein in L1210/VCR cells is associated with changes in several endoplasmic reticulum proteins that may be partially responsible for the lack of thapsigargin sensitivity. *Gen. Physiol. Biophys.* **27**, 211-221 (2008).
90 Sulová, Z. *et al.* Expression of P-glycoprotein in L1210 cells is linked with rise in sensitivity to Ca^{2+}. *Biochem. Biophys. Res. Comm.* **335**, 777-784 (2005).
91 Michelangeli, F. & East, J. A diversity of SERCA Ca^{2+} pump inhibitors. *Biochem. Soc. Trans.* **39**, 789-886 (2011).
92 Treiman, M., Caspersen, C. & Christensen, S. A tool coming of age: thapsigargin as an inhibitor of sarco-endoplasmic reticulum Ca^{2+}-ATPases. *Trends Pharmacol. Sci.* **19**, 131-136 (1998).
93 Cheng, T. & Benton, H. The intracellular Ca^{2+}-pump inhibitors thapsigargin and cyclopiazonic acid induce stress proteins in mammalian chondrocytes. *Biochem. J.* **301**, 563-571 (1994).
94 Olesen, C. *et al.* The structural basis of calcium transport by the calcium pump. *Nature* **450**, 1036-1078 (2007).

95 Takahashi, M., Kondou, Y. & Toyoshima, C. Interdomain communication in calcium pump as revealed in the crystal structures with transmembrane inhibitors. *Proc. Natl. Acad. Sci.* **104**, 5800-5805 (2007).
96 Winther, A.-M. L. *et al.* Critical roles of hydrophobicity and orientation of side chains for inactivation of sarcoplasmic reticulum Ca^{2+}-ATPase with thapsigargin and thapsigargin analogs. *J. Biol. Chem.* **285**, 28883-28975 (2010).
97 Seidler, N., Jona, I., Vegh, M. & Martonosi, A. Cyclopiazonic acid is a specific inhibitor of the Ca^{2+}-ATPase of sarcoplasmic reticulum. *J. Biol. Chem.* **264**, 17816-17839 (1989).
98 Khan, Y., Wictome, M., East, J. & Lee, A. Interactions of dihydroxybenzenes with the Ca^{2+}-ATPase: separate binding sites for dihydroxybenzenes and sesquiterpene lactones. *Biochemistry* **34**, 14385-14478 (1995).
99 Ghantous, A., Gali-Muhtasib, H., Vuorela, H., Saliba, N. A. & Darwiche, N. What made sesquiterpene lactones reach cancer clinical trials? *Drug Discov. Today* **15**, 668-678 (2010).
100 Denmeade, S. *et al.* Prostate-specific antigen-activated thapsigargin prodrug as targeted therapy for prostate cancer. *J. Natl. Cancer Inst.* **95**, 990-1000 (2003).
101 Denmeade, S. & Isaacs, J. The SERCA pump as a therapeutic target: making a "smart bomb" for prostate cancer. *Cancer Biol. Ther.* **4**, 14-22 (2005).
102 Roti, G. *et al.* Complementary genomic screens identify SERCA as a therapeutic target in NOTCH1 mutated cancer. *Cancer Cell* **23**, 390-405 (2013).
103 Wang, J.-L. *et al.* Structure-based discovery of an organic compound that binds Bcl-2 protein and induces apoptosis of tumor cells. *Proc. Natl. Acad. Sci.* **97**, 7124-7129 (2000).
104 Doshi, J., Tian, D. & Xing, C. Structure-activity relationship studies of ethyl 2-amino-6-bromo-4-(1-cyano-2-ethoxy-2-oxoethyl)-4*H*-chromene-3-carboxylate (HA 14-1), an antagonist for antiapoptotic Bcl-2 proteins to overcome drug resistance in cancer. *J. Med. Chem.* **49**, 7731-7739 (2006).
105 Das, S. *et al.* Structure-activity relationship and molecular mechanisms of ethyl 2-amino-4-(2-ethoxy-2-oxoethyl)-6-phenyl-4*H*-chromene-3-carboxylate (sha 14-1) and its analogues. *J. Med. Chem.* **52**, 5937-5949 (2009).
106 Hermanson, D. *et al.* Dual mechanisms of sHA 14-1 in inducing cell death through endoplasmic reticulum and mitochondria. *Mol. Pharmacol.* **76**, 667-745 (2009).
107 Tian, D. *et al.* sHA 14-1, a stable and ROS-free antagonist against anti-apoptotic Bcl-2 proteins, bypasses drug resistances and synergizes cancer therapies in human leukemia cell. *Cancer Lett.* **259**, 198-208 (2008).
108 Das, S. *et al.* Structure-activity relationship and molecular mechanisms of ethyl 2-amino-6-(3,5-dimethoxyphenyl)-4-(2-ethoxy-2-oxoethyl)-4*H*-chromene-3-carboxylate (CXL017) and its analogues. *J. Med. Chem.* **54**, 5937-5985 (2011).
109 Das, S. *et al.* Ethyl 2-Amino-6-(3,5-dimethoxyphenyl)-4-(2-ethoxy-2-oxoethyl)-4*H*-chromene-3-carboxylate (CXL017): a novel scaffold that resensitizes multidrug resistant leukemia cells to chemotherapy. *ACS Chem. Biol.* **8**, 327-335 (2013).

110 Curini, M. *et al*. Preparation of 2-amino-4*H*-chromene derivatives from coumarins in basic media. *Eur. J. Org. Chem.* **2006**, 746-751 (2006).
111 Vaziri, S. *et al.* c-IAP1 is overexpressed in HL-60 cells selected for doxorubicin resistance: effects on etoposide-induced apoptosis. *Anticancer Res.* **23**, 3657-3661 (2003).
112 Harker, W., Slade, D., Drake, F. & Parr, R. Mitoxantrone resistance in HL-60 leukemia cells: reduced nuclear topoisomerase II catalytic activity and drug-induced DNA cleavage in association with reduced expression of the topoisomerase II beta isoform. *Biochemistry* **30**, 9953-9961 (1991).
113 Harker, W., Slade, D., Dalton, W., Meltzer, P. & Trent, J. Multidrug resistance in mitoxantrone-selected HL-60 leukemia cells in the absence of P-glycoprotein overexpression. *Cancer Res.* **49**, 4542-4549 (1989).
114 Fujimori, A., Harker, W., Kohlhagen, G., Hoki, Y. & Pommier, Y. Mutation at the catalytic site of topoisomerase I in CEM/C2, a human leukemia cell line resistant to camptothecin. *Cancer Res.* **55**, 1339-1346 (1995).
115 Fujimori, A., Hoki, Y., Popescu, N. & Pommier, Y. Silencing and selective methylation of the normal topoisomerase I gene in camptothecin-resistant CEM/C2 human leukemia cells. *Oncol. Res.* **8**, 295-301 (1996).
116 Chen, M. & Beck, W. DNA topoisomerase II expression, stability, and phosphorylation in two VM-26-resistant human leukemic CEM sublines. *Oncol. Res.* **7**, 103-111 (1995).
117 Beck, W., Mueller, T. & Tanzer, L. Altered surface membrane glycoproteins in vinca alkaloid-resistant human leukemic lymphoblasts. *Cancer Res.* **39**, 2070-2076 (1979).
118 Tang, R. *et al.* P-gp activity is a critical resistance factor against AVE9633 and DM4 cytotoxicity in leukaemia cell lines, but not a major mechanism of chemoresistance in cells from acute myeloid leukaemia patients. *BMC Cancer* **9**, 199 (2009).
119 Cai, J. *et al.* Two distinct molecular mechanisms underlying cytarabine resistance in human leukemic cells. *Cancer Res.* **68**, 2349-2357 (2008).
120 Kapoor, R., Slade, D., Fujimori, A., Pommier, Y. & Harker, W. Altered topoisomerase I expression in two subclones of human CEM leukemia selected for resistance to camptothecin. *Oncol. Res.* **7**, 83-95 (1995).
121 Toyoshima, C. & Nomura, H. Structural changes in the calcium pump accompanying the dissociation of calcium. *Nature* **418**, 605-616 (2002).
122 Inesi, G., Lewis, D., Ma, H., Prasad, A. & Toyoshima, C. Concerted conformational effects of Ca^{2+} and ATP are required for activation of sequential reactions in the Ca^{2+} ATPase (SERCA) catalytic cycle. *Biochemistry* **45**, 13769-13847 (2006).
123 Bilmen, J., Khan, S., Javed, M. & Michelangeli, F. Inhibition of the SERCA Ca^{2+} pumps by curcumin. Curcumin putatively stabilizes the interaction between the nucleotide-binding and phosphorylation domains in the absence of ATP. *Eur. J. Biochem.* **268**, 6318-6327 (2001).

124 Chene, P. ATPases as drug targets: learning from their structure. *Nat. Rev. Drug Discov.* **1**, 665-673 (2002).
125 Mueller, B., Zhao, M., Negrashov, I., Bennett, R. & Thomas, D. SERCA structural dynamics induced by ATP and calcium. *Biochemistry* **43**, 12846-12854 (2004).
126 Aridoss, G., Zhou, B., Hermanson, D. L., Bleeker, N. P. & Xing, C. Structure–activity relationship (SAR) study of ethyl 2-amino-6-(3,5-dimethoxyphenyl)-4-(2-ethoxy-2-oxoethyl)-4*H*-chromene-3-carboxylate (CXL017) and the potential of the lead against multidrug resistance in cancer treatment. *J. Med. Chem.* **55**, 5566-5581 (2012).
127 Chou, T.-C. Drug combination studies and their synergy quantification using the Chou-Talalay method. *Cancer Res.* **70**, 440-446 (2010).
128 Jia, J. *et al.* Mechanisms of drug combinations: interaction and network perspectives. *Nat. Rev. Drug Discov.* **8**, 111-139 (2009).
129 Chou, T., Motzer, R., Tong, Y. & Bosl, G. Computerized quantitation of synergism and antagonism of taxol, topotecan, and cisplatin against human teratocarcinoma cell growth: a rational approach to clinical protocol design. *J. Natl. Cancer Inst.* **86**, 1517-1541 (1994).
130 Winters, D., Autry, J., Svensson, B. & Thomas, D. Interdomain fluorescence resonance energy transfer in SERCA probed by cyan-fluorescent protein fused to the actuator domain. *Biochemistry* **47**, 4246-4302 (2008).
131 Chou, T. & Talalay, P. Quantitative analysis of dose-effect relationships: the combined effects of multiple drugs or enzyme inhibitors. *Adv. Enzyme Regul.* **22**, 27-82 (1984).
132 Ziegler, S., Pries, V., Hedberg, C. & Waldmann, H. Target identification for small bioactive molecules: finding the needle in the haystack. *Angew. Chem. Int. Ed.* **52**, 2744-2792 (2013).
133 Robinette, D., Neamati, N., Tomer, K. B. & Borchers, C. H. Photoaffinity labeling combined with mass spectrometric approaches as a tool for structural proteomics. *Expert Rev. Proteomics* **3**, 399-408 (2006).
134 Vodovozova, E. L. Photoaffinity labeling and its application in structural biology. *Biochemistry (Moscow)* **72**, 1-20 (2007).
135 Colca, J. & Harrigan, G. Photo-affinity labeling strategies in identifying the protein ligands of bioactive small molecules: examples of targeted synthesis of drug analog photoprobes. *Comb. Chem. High Throughput Screen.* **7**, 699-704 (2004).
136 Geurink, P., Prely, L., van der Marel, G., Bischoff, R. & Overkleeft, H. Photoaffinity labeling in activity-based protein profiling. *Topics Curr. Chem.* **324**, 85-113 (2012).
137 Köcher, T. & Superti-Furga, G. Mass spectrometry-based functional proteomics: from molecular machines to protein networks. *Nature Methods* **4**, 807-815 (2007).
138 Speers, A. E. & Cravatt, B. F. Chemical strategies for activity-based proteomics. *ChemBioChem* **5**, 41-47 (2004).

139 Kolb, H. C., Finn, M. G. & Sharpless, K. B. Click chemistry: diverse chemical function from a few good reactions. *Angew. Chem. Int. Ed.* **40**, 2004-2021 (2001).
140 Himo, F. *et al.* Copper(I)-catalyzed synthesis of azoles. DFT study predicts unprecedented reactivity and intermediates. *J. Am. Chem. Soc.* **127**, 210-216 (2004).
141 Best, M. D. Click chemistry and bioorthogonal reactions: unprecedented selectivity in the labeling of biological molecules. *Biochemistry* **48**, 6571-6584 (2009).
142 Thirumurugan, P., Matosiuk, D. & Jozwiak, K. Click chemistry for drug development and diverse chemical–biology applications. *Chem. Rev.* **113**, 4905-4979 (2013).
143 Barral, K., Moorhouse, A. D. & Moses, J. E. Efficient conversion of aromatic amines into azides: a one-pot synthesis of triazole linkages. *Org. Lett.* **9**, 1809-1811 (2007).
144 Stokes, D. & Green, N. Three-dimensional crystals of CaATPase from sarcoplasmic reticulum. Symmetry and molecular packing. *Biophys. J.* **57**, 1-14 (1990).